Synaptotagmin 9 modulates spontaneous neurotransmitter release in striatal neurons by regulating substance P secretion

Michael J. Seibert,[1,2] Chantell S. Evans,[3] Kevin S. Stanley,[1] Zhenyong Wu,[1] and Edwin R. Chapman[1*]

[1] Howard Hughes Medical Institute and Department of Neuroscience, University of Wisconsin-Madison School of Medicine and Public Health, Madison, WI, 53705, USA

[2] Neuroscience Training Program, University of Wisconsin-Madison School of Medicine and Public Health, Madison, WI, 53705, USA

[3] Department of Cell Biology, Duke University School of Medicine, Durham, NC, 27710, USA

* Corresponding author: E-mail: chapman@wisc.edu

ABSTRACT

Synaptotagmin 9 (SYT9) is a tandem C2-domain Ca^{2+} sensor for exocytosis in neuroendocrine cells; its function in neurons remains unclear. Here, we show that endogenous SYT9 does not trigger rapid synaptic vesicle exocytosis in cultured cortical, hippocampal, or striatal neurons; rather, synaptotagmin 1 (SYT1) fulfills this function. SYT9 is able to regulate evoked synaptic vesicle exocytosis, but only when massively over-expressed. In striatal neurons, loss of SYT9 reduced the rate of spontaneous miniature neurotransmitter release events (minis). To delve into the underlying mechanism, we localized SYT9 within these neurons and found that it is targeted to dense core vesicles, where it regulates the release of substance P (SP), a neuropeptide known to modulate mini frequency. Exogenous SP, but not other striatal peptide hormones, completely rescued the *Syt9* KO mini phenotype. Biochemical experiments revealed that Ca^{2+}-binding to the C2A domain of SYT9 triggers membrane fusion *in vitro*, and mutations that disrupt this activity abolished the ability of SYT9 to regulate both SP

release and mini frequency in striatal neurons. We conclude that SYT9 indirectly regulates synaptic transmission in striatal neurons by controlling SP release.

INTRODUCTION

The synaptotagmins (SYTs) are a large family of membrane trafficking proteins; seventeen isoforms have been identified in mammals, each encoded by a distinct gene (Craxton, 2010; Wolfes & Dean, 2020). In addition, most isoforms are thought to undergo alternative splicing, generating further potential diversity within this family (Craxton, 2010). Most isoforms have a single N-terminal transmembrane domain (TMD) with a short intra-luminal domain. In all isoforms, the cytoplasmic domain largely comprises tandem C2-domains that are connected by a short linker. In at least eight of the seventeen isoforms, the C2-domains serve as Ca^{2+}-dependent anionic lipid-binding motifs (Bhalla et al., 2008; Rickman et al., 2004). Ca^{2+} binding is thought to be mediated by acidic side chains in two flexible loops that protrude from each C2-domain (Sutton et al., 1995). In the case of SYT1, Ca^{2+} triggers the partial penetration of these loops into lipid bilayers and facilitates interactions with SNARE proteins (Chapman, 2008). While membrane penetration is an essential step in Ca^{2+}-triggered exocytosis (Bai et al., 2016; Evans et al., 2015; Liu et al., 2014), the role of SYT-SNARE interactions in membrane fusion remains unresolved (Bai et al., 2016; Bhalla et al., 2006; Chicka et al., 2008; Das et al., 2020; Van Den Bogaart et al., 2011; Zhou et al., 2017).

A current goal is to understand the functional diversity within the SYT family of proteins. SYT1 and SYT2 have been heavily studied and shown to serve as Ca^{2+} sensors that trigger rapid, synchronous synaptic vesicle (SV) exocytosis in neurons (Geppert et al., 1994; Pang, Melicoff, et al., 2006; Stevens & Sullivan, 2003). SYT1 also regulates SV docking (Chang et al., 2018; Liu et al., 2009; Reist et al., 1998), endocytosis (Jorgensen et al., 1995; Nicholson-Tomishima & Ryan, 2004; Poskanzer et al., 2003; Yao et al., 2012), and spontaneous release (Bai et al., 2016; Courtney et al., 2019; DiAntonio & Schwarz, 1994; Kerr et al., 2008; Littleton et

53 al., 1994; Vevea & Chapman, 2020). Importantly, SYT1 and SYT2 form a closely related clade
54 with one more family member, SYT9 (Rickman et al., 2004). This homology prompted the idea
55 that SYT9 might also function as a fast Ca^{2+} sensor for SV release, which is a point we address
56 in detail in the current study. For clarity, we note that SYT9 is sometimes referred to as SYT5,
57 and vice versa; the SYT9 studied here comprises 386 residues (NCBI Gene accession # 53420)
58 whereas SYT5 is 491 residues in length (NCBI Gene accession #60510).

59 Along with SYT1, SYT9 co-regulates catecholamine secretion from dense core vesicles
60 (DCV) in PC12 cells (Fukuda et al., 2002; Lynch & Martin, 2007). SYT9 also regulates the
61 release of follicle-stimulating hormone (FSH) from DCVs in the gonadotrophs of female mice in
62 a sex-specific manner (Roper et al., 2015). However, while SYT9 is widely expressed in the
63 brain ([Mittelsteadt et al., 2009]; note: these authors referred to SYT9 as SYT5), its function in
64 neurons remains controversial. One report concluded that SYT9 serves as a Ca^{2+} sensor for
65 rapid SV exocytosis in cultured striatal neurons (Xu et al., 2007). In contrast, SYT9 failed to
66 support SV exocytosis in *Syt1* KO hippocampal neurons, and pHluorin-tagged SYT9 underwent
67 regulated exocytosis in both axons and dendrites of hippocampal neurons, with kinetics
68 suggestive of DCV fusion (Dean, Dunning, et al., 2012).

69 To address and clarify the function of SYT9 in neurons, we studied synaptic
70 transmission in cultured hippocampal, cortical, and striatal neurons obtained from *Syt9* KO
71 mice; for completeness *Syt1* KO neurons were examined in parallel. We show that all three
72 classes of neurons express both SYT9 and SYT1, but loss of SYT9 had no discernable effect
73 on evoked neurotransmitter release, while loss of SYT1 disrupted rapid transmission in all three
74 neuronal preparations. SYT9 was able to rescue the loss of synchronous release that is
75 characteristic of *Syt1* KO neurons, but only when over-expressed by ~25-fold, which matched
76 the expression levels of endogenous SYT1. Interestingly, loss of SYT9 in cultured striatal
77 neurons resulted in a specific and unexpected phenotype: a decrease in the spontaneous
78 miniature SV fusion rate (i.e., mini frequency). We then discovered that SYT9 was co-localized

79 with substance P (SP), a DCV peptide hormone known to be enriched in striatal neurons.
80 Moreover, loss of SYT9 impaired action potential-triggered SP release. Importantly, in patch-
81 clamp experiments, supplementing the bath with this neuropeptide rescued the mini phenotype.
82 Moreover, the structural elements of Syt9 that underlie Ca^{2+} triggered membrane fusion *in vitro*
83 also support evoked SP release and spontaneous SV fusion in living striatal neurons. These
84 findings reveal a mechanism in which SYT9 indirectly regulates spontaneous transmission in
85 striatal neurons by directly regulating secretion of the neuromodulator, SP.
86

87 **RESULTS**

88 **Synaptotagmin 9 is not required for fast, synchronous neurotransmitter release in**
89 **cultured neurons**

90 Immunoblot analysis of neuronal culture lysates revealed that SYT1 and SYT9 are
91 expressed in cortical, hippocampal, and striatal neurons (**Fig. 1a,e**). By including known
92 amounts of purified recombinant SYT1 cytoplasmic domain (C2AB) or SYT9 (full-length) as
93 standards on these blots we were able to determine the absolute expression levels via
94 quantitative densitometry (**Fig. 1b,f**). This analysis revealed that SYT1 and SYT9 were ~0.1%
95 and ~0.004% of the total protein in each of the neuronal lysates, respectively. Hence, SYT1
96 expression is ~25 times greater than SYT9 in all three classes of neurons.

97 A prior study suggested that SYT1 and SYT9 serve as partially redundant Ca^{2+} sensors
98 in striatal neurons and that SYT9 can fully rescue fast release in *Syt1* KO cortical neurons (Xu
99 et al., 2007). However, this is difficult to reconcile with the well-established findings that loss of
100 SYT1 in hippocampal and cortical neurons disrupts virtually all synchronous release (Geppert et
101 al., 1994; Maximov & Südhof, 2005). If SYT9 is a sensor for synchronous release, some fast
102 release should have persisted in the *Syt1* KO neurons. To address this conundrum, whole-cell
103 patch-clamp experiments were conducted using cultured neurons from *Syt1* conditional KO
104 (cKO) and *Syt9* KO mice. In striatal *Syt1* cKO neurons, ablation of SYT1 expression with

application of CRE lentivirus eliminated fast, synchronous neurotransmitter release with an 8-fold reduction in evoked inhibitory postsynaptic current (eIPSC) amplitude (**Fig. 1c,d**). Disruption of SYT9 expression, however, did not result in any change in eIPSC amplitude or kinetics in striatal neurons (**Fig. 1g,h**). Analogous results were obtained using cultured cortical and hippocampal neurons (**Supp. Fig. 1**). Evoked release during a stimulus train was also unaffected in *Syt9* KO cortical, hippocampal, and striatal neurons, further demonstrating that this isoform does not impact evoked transmission (**Supp. Fig. 2**). We conclude that endogenous SYT9 is unable to support synchronous release in absence of SYT1 in any of the neuronal preparations studied here, perhaps because of the relatively low expression levels of this protein.

Figure 1

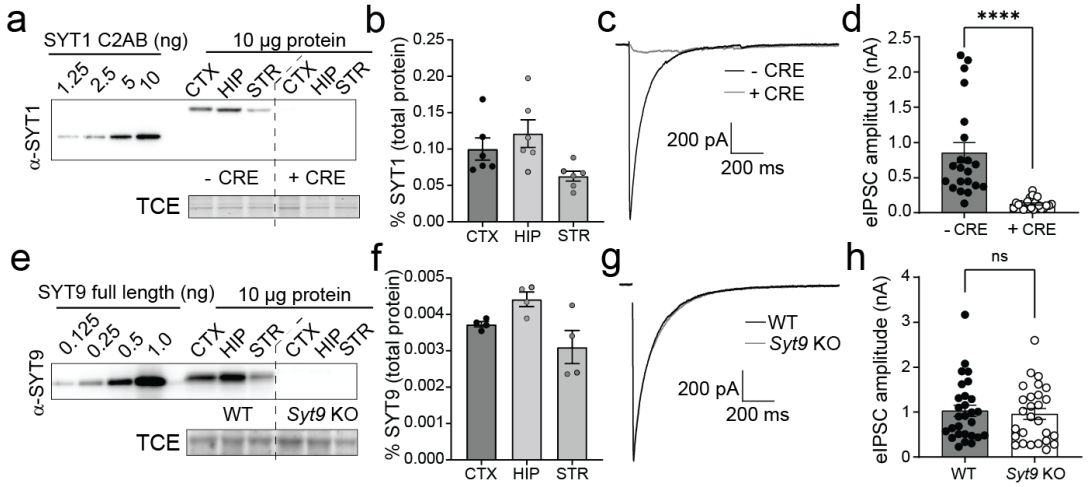

Figure 1. SYT9 is expressed in cultured cortical, hippocampal, and striatal neurons but does not support evoked neurotransmitter release. a, Immunoblot of day *in vitro* (DIV) 14 cortical (CTX), hippocampal (HIP), and striatal (STR) neuronal lysates from *Syt1* cKO neurons +/- CRE virus; recombinant SYT1 C2AB served as a standard to quantify SYT1 expression levels. TCE staining served as a loading control. **b**, Quantification of the SYT1 expression levels in each of the three neuronal lysates, as a fraction of total protein (n = 6). **c**, Averaged evoked IPSC (eIPSC) traces from *Syt1* cKO striatal neurons +/- CRE, and (**d**) peak eIPSC amplitudes from - CRE (n = 21) or + CRE (n = 22) cells, showing loss of synchronous release upon loss of

127 SYT1 ($p < 0.0001$; Mann-Whitney test). **e**, Same as panel (**a**) but blotting for SYT9 in lysates
128 from WT and *Syt9* KO striatal neurons, using the indicated amounts of a full-length recombinant
129 SYT9 standard. **f**, Same as panel (**b**), but for SYT9 expression in WT and *Syt9* KO striatal
130 neurons (n = 4); SYT9 is expressed at ~25-fold lower levels than SYT1. **g**-**h**, Same as panels
131 (**c**-**d**), but in WT (n = 28) and *Syt9* KO (n = 27) striatal neurons. In sharp contrast to *Syt1* cKO +
132 CRE neurons, loss of SYT9 did not affect single eIPSCs in striatal neurons ($p = 0.6979$;
133 unpaired Student's t-test). ****$p < 0.0001$; ns indicates $p > 0.05$, and error bars represent SEM.
134

135 **SYT9 rescues SYT1 KO phenotypes only when over-expressed**

136 Xu et al. (2007) reported that SYT9 over-expression can functionally rescue
137 synchronous neurotransmitter release in cultured *Syt1* KO cortical neurons (Xu et al., 2007).
138 Similar observations were made upon over-expression of SYT9 in a calyx of Held slice
139 preparation lacking the primary Ca^{2+} sensor at this synapse, SYT2 (Kochubey et al., 2016).
140 Given the observation that endogenous SYT9 is expressed at levels ~25-fold lower than SYT1
141 (**Fig. 1b,f**), a quantitative approach was taken to re-evaluate this previously reported rescue
142 activity. Cultured *Syt1* cKO cortical neurons were treated at DIV1 with a CRE lentivirus to
143 disrupt SYT1 expression and then transduced at DIV5 with lentivirus to express SYT9 with an
144 N-terminal pHluorin tag (pH-SYT9). The pH-SYT9 lentivirus was titered such that expression of
145 pH-SYT9 in the + CRE neurons would be either 1x or 25x the endogenous SYT9 expression
146 level; the latter condition matching the levels of endogenous SYT1 (**Fig. 2a**; **Fig. 1**). Ablation of
147 SYT1 expression again resulted in a loss of fast, synchronous neurotransmission, and 1x over-
148 expression of pH-SYT9 had no significant effect on eIPSC amplitude, and while there was a
149 decrease in the time-to-peak this did not reach significance (**Fig. 2b-d**). However, 25x over-
150 expression of pH-SYT9 significantly rescued the eIPSC amplitude (60% compared to - CRE)
151 and completely rescued the eIPSC time-to-peak (**Fig. 2b-d**). The 25x over-expression condition
152 also rescued the decay time of the + CRE condition (**Supp. Fig. 3**). So, only supraphysiological
153 SYT9 expression levels rescue evoked responses in neurons lacking SYT1 (Kochubey et al.,
154 2016; Xu et al., 2007).

155 SYT1 is a multifunctional protein that also serves to clamp spontaneous neurotransmitter
156 release under resting conditions (Bai et al., 2016; Chicka et al., 2008; Courtney et al., 2019; Liu
157 et al., 2014; Vevea & Chapman, 2020). To investigate whether over-expressed pH-SYT9 can
158 clamp spontaneous fusion, miniature inhibitory postsynaptic currents (mIPSCs, also called
159 minis) were recorded in the presence of tetrodotoxin, to block action potentials (**Fig. 2e**).
160 Disruption of SYT1 resulted in a ~3-fold increase in mIPSC frequency with no rescue observed
161 in the 1x pH-SYT9 over-expression condition. In contrast, 25x over-expression of SYT9 resulted
162 in a complete rescue of clamping activity (**Fig. 2f**). mIPSC amplitude and rise and decay kinetics
163 were unaffected across conditions (data not shown). Taken together, these findings indicate that
164 SYT9 can rescue evoked release and clamp spontaneous release, in *Syt1* KO neurons, only
165 when massively over-expressed.
166 To investigate how the localization of over-expressed SYT9 functions to support SV
167 release, we utilized the N-terminal pHluorin tag to differentiate between pools in the plasma
168 membrane versus internal compartments (see Methods and [Courtney et al., 2019]). We co-
169 stained with antibodies against synaptophysin (SYP), to label SVs. The internal fraction in the
170 1x over-expression condition showed some degree of colocalization with SYP, and the internal
171 fraction of 25x pH-SYT9 had a higher degree of colocalization. We note that endogenous SYT9
172 colocalized with SYP to a similar degree as 1x over-expressed pH-SYT9, while 25x over-
173 expressed pH-SYT9 colocalized with SYP to a similar degree as endogenous SYT1 (**Fig. 2h, i**).
174 These results are congruent with the idea that some SYT9 may be present on SVs, as indicated
175 in proteomic studies (Takamori et al., 2006; Taoufiq et al., 2020). However, these levels are too
176 low to support evoked release or to clamp spontaneous release, at least in the types of neurons
177 studied here.
178
179 **Figure 2**

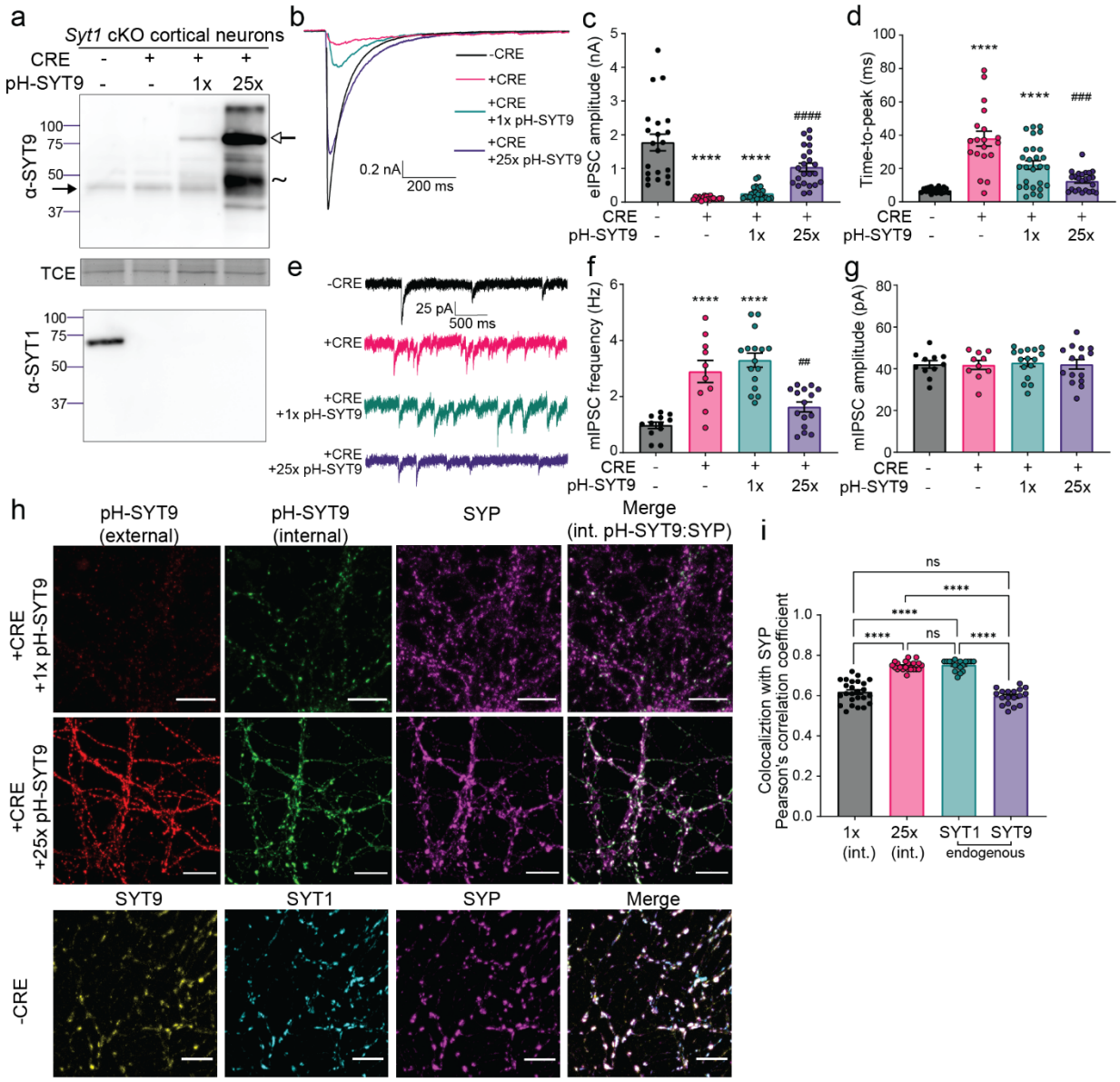

Figure 2. SYT9 rescues SYT1 KO phenotypes only when over-expressed. a, Immunoblots of DIV14 cortical neuronal lysates from *Syt1* cKO mice, with or without addition of CRE lentivirus. TCE staining served as a loading control (note: in all trials the α-SYT9 blot was stripped and re-probed with an α-SYT1 antibody, so TCE control is shown only once). + CRE neurons were later transduced with lentivirus encoding pHluorin-tagged SYT9 (pH-SYT9), resulting in either a 1x or 25x degree of over-expression as compared to endogenous SYT9. The closed arrowhead indicates endogenous SYT9, the open arrowhead indicates pH-SYT9, and the ~ indicates proteolytic fragments from pH-SYT9. Averaged eIPSC traces (**b**), amplitudes (**c**), and time-to-peak for each condition (**d**), are plotted for - CRE (n = 21), + CRE (n = 19), + CRE +1x pH-SYT9 (n = 25), and + CRE +25x pH-SYT9 (n = 23) conditions. SYT9 partially rescued eIPSC amplitude and time-to-peak, but only when over-expressed 25-fold. **e**, Representative miniature IPSC (mIPSC) traces, showing increased rates of mIPSCs in *Syt1*

193 cKO + CRE (n = 10) neurons compared to - CRE (n = 12). 1x over-expression of SYT9 was
194 without effect (n = 16); full rescue of the unclamped phenotype was observed at 25x over-
195 expression (n = 15); these data are quantified in (**f**). **g**, mIPSC amplitude was unaffected under
196 all conditions. **h**, Representative immunofluorescence images of cultured *Syt1* cKO cortical
197 neurons +/- CRE, with and without over-expressed pH-SYT9. Rescue constructs were tagged at
198 the N-terminus with a pHluorin to enable differential labeling of the surface and internal fractions
199 using α-GFP antibodies, see Methods for details. pH-SYT9 was present in both the plasma
200 membrane (red) and on internal compartments (green). SVs were marked using an α-
201 synaptophysin (SYP) antibody (magenta). **i**, Quantification of the colocalization between
202 synaptophysin and: internal pH-SYT9, endogenous SYT1, and endogenous SYT9. In **c**-**g**,
203 asterisks (*) indicate statistical comparisons (one-way ANOVA with Šídák's multiple
204 comparisons test) to *Syt1* cKO neurons without CRE, where ****$p < 0.0001$; hash symbols (#)
205 indicate statistical comparisons to *Syt1* cKO neurons + CRE, where ##$p < 0.01$; and ###$p <$
206 0.001; and ####$p < 0.0001$.
207

208 **Decreased mIPSC frequency in SYT9 KO striatal neurons**

209 To further characterize neurotransmission in *Syt9* KO mice, spontaneous release from
210 cultured striatal neurons was measured and compared to WT controls. We reiterate that all
211 aspects of release evoked by single action potentials were normal (**Fig. 1g**); however, the
212 mIPSC frequency in *Syt9* KO striatal neurons was reduced 2-fold (**Fig. 3a,c**), with no effect on
213 the amplitude or kinetics of these spontaneous quantal events (**Fig. 3b**). Interestingly, when the
214 same experiment was performed using cortical and hippocampal neurons, loss of SYT9 did not
215 affect spontaneous release rates (**Supp. Fig. 4**), suggesting that this phenotype was specific for
216 striatal neurons, most of which are GABAergic medium spiny neurons (MSNs) (Kemp & Powell,
217 1971). Importantly, the density of synapses was unchanged between WT and *Syt9* KO striatal
218 neurons (**Supp. Fig. 5**).

219 We note that most mIPSCs are Ca^{2+}-dependent and are thought to use the same Ca^{2+}
220 sensors as evoked synchronous and asynchronous release, including SYT1 and Doc2
221 (Courtney et al., 2018; Groffen et al., 2010; Xu et al., 2009). The insufficiency of endogenous
222 SYT9 to drive evoked release argues against the idea that it is a Ca^{2+} sensor for mIPSCs.
223 Furthermore, the specificity of the mIPSC phenotype for striatal versus hippocampal or cortical
224 neurons suggests a cell-specific mechanism for the action of SYT9 in spontaneous release.

225 Notably, SYT9 is targeted to DCVs in a variety of tissues (Fukuda et al., 2002; Iezzi et al., 2005;
226 Lynch & Martin, 2007; Roper et al., 2015), and some DCV neuropeptides have been shown to
227 regulate aspects of synaptic transmission (Cao et al., 2011; Dean et al., 2009; He et al., 2019).
228 This prompts the idea that SYT9 might regulate minis indirectly, potentially by controlling the
229 release of neuromodulators from DCVs.

230

231 **Figure 3**

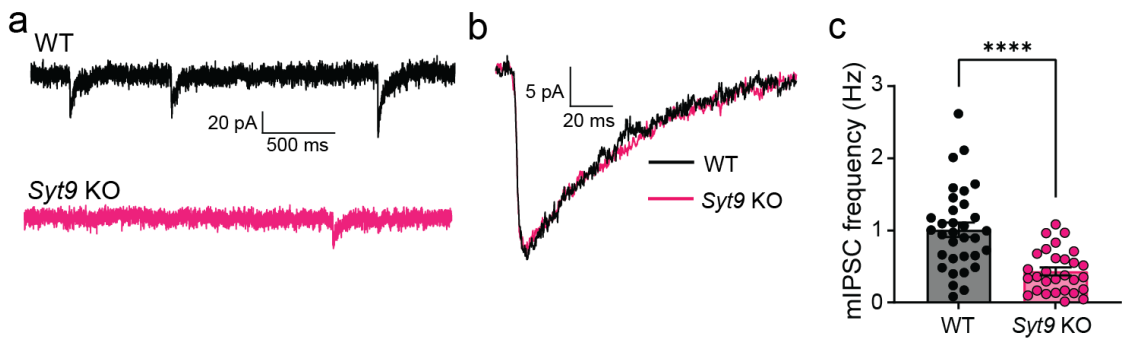

232

233 **Figure 3. SYT9 KO striatal neurons display decreased mIPSC frequency. a**, Representative
234 mIPSCs traces recorded from WT (n = 33) and *Syt9* KO (n = 29) striatal neurons. **b**, Overlay of
235 averaged mIPSCs from the two above conditions, revealing no change in kinetics or amplitude.
236 **c**, mIPSC frequency is reduced in *Syt9* KO striatal neurons ($p < 0.0001$; Welch's t-test).
237

238 **SYT9 regulates the secretion of substance P-pHluorin from striatal neurons**

239 To investigate the mechanism by which SYT9 regulates mIPSC frequency, we
240 conducted further localization studies. Since the *Syt9* KO phenotype was specific for striatal
241 neurons, we focused on striatum-specific DCV neuropeptides. Among these, substance P (SP)
242 was of particular interest because it has been shown to regulate mIPSC frequency in striatal
243 neurons through its action on the neurokinin 1 receptor (NK1R) (He et al., 2019). Interestingly,
244 SP is not enriched in hippocampal or cortical neurons (Shults et al., 1984), where the mIPSC
245 phenotype was not observed.

246 Specific antibodies for SP are not available, so we transduced striatal neurons with a
247 lentivirus that expresses an SP-pHluorin (SP-pH) fusion protein and performed
248 immunocytochemistry (ICC) to assess co-localization of the pHluorin tag with endogenous
249 SYT9. Strikingly, SYT9 was colocalized with SP-pH (**Fig. 4a,b**). The correct localization of the
250 SP-pH construct was confirmed by staining for chromogranin B (CHGB), a canonical DCV
251 marker in neurons (**Fig. 4c,d**). In summary, these findings demonstrate the presence of SYT9
252 on DCVs that bear a neuropeptide known to regulate mIPSC frequency (He et al., 2019)
253 Next, we sought to determine whether SYT9 regulates SP release from DCVs in striatal
254 neurons. To optically measure SP secretion events at single-event resolution, WT and *Syt9* KO
255 neurons were sparsely transfected with a plasmid encoding SP-pH to enable imaging of
256 individual neurons. SP-pH fluorescence is quenched in the low pH environment of the DCV
257 lumen; upon exocytosis, the pHluorin is rapidly dequenched, yielding a robust increase in
258 fluorescence intensity (**Fig. 4e**). In cultured neurons, repetitive high-frequency electrical
259 stimulation (i.e.,16 bursts of 50 APs at 50Hz) has been shown to effectively trigger these
260 release events (Persoon et al., 2018); this paradigm was used in our experiments and yielded
261 robust exocytosis (**Fig. 4f; Video 1**). DCV fusion was quantified in WT and *Syt9* KO striatal
262 neurons, where the released fraction was calculated as the number of fusion events divided by
263 the total number of SP-pH vesicles in a single neuron. The total SP-pH DCV pool was estimated
264 by perfusing neurons with NH_4Cl to alkalinize the lumen of DCVs and dequench the pHluorin
265 reporter; no significant differences were observed between the WT and *Syt9* KO (**Fig 4g**). In WT
266 neurons the released fraction was ~10%. In *Syt9* KO neurons this was reduced by ~61% (**Fig.
267 4h, i**), with only ~3.9% of the vesicles being released. Fusion event duration was also measured
268 in WT and *Syt9* KO neurons, and there appeared to be a small population of long-duration
269 release events that was absent in the WT (**Fig. 4j**), hinting at a potential role of SYT9 in
270 regulating the fate of fusion pores, as shown for other SYT isoforms (Rao et al., 2014; Wang et
271 al., 2001). Finally, loss of SYT9 had no apparent effect on the transport of SP-pH vesicles,

272 suggesting that the observed reductions in SP secretion were not secondary to trafficking

273 defects (**Supp. Fig. 6**).

274

275 **Figure 4**

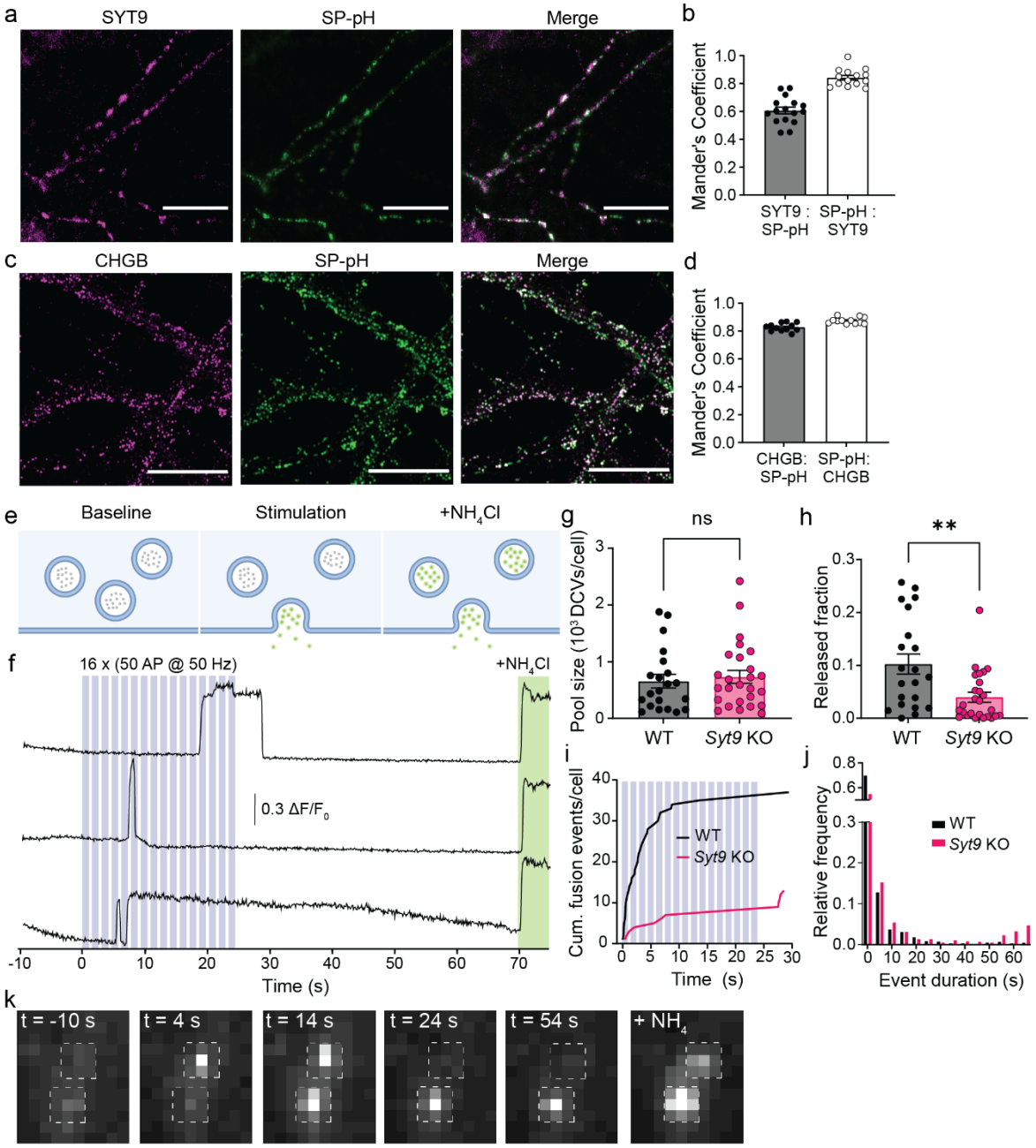

276

277 **Figure 4. SYT9 regulates the secretion of substance P-pHluorin from striatal neurons. a**,
278 Representative images of cultured striatal neurons stained with α-SYT9 (magenta) and α-GFP
279 (SP-pH) (green) antibodies; channels are merged on the right. **b**, SYT9 is co-localized with SP-

280 pH, and vice versa; quantification was conducted using the Mander's overlap coefficient. **c**-**d**, As
281 in panels (**a**-**b**) but co-stained with α-CHGB (magenta) and α-GFP antibodies (green). SP-pH is
282 co-localized with CHGB, confirming that SP-pH is targeted to DCVs. **e**, Schematic of the SP-pH
283 release assay. **f**, Representative traces of individual SP-pH vesicle fusion events; the
284 stimulation paradigm is overlaid in blue, and alkalinization of DCVs with NH_4Cl is shown in
285 green. **g**, Pool size per neuron was unchanged in *Syt9* KO neurons ($p = 0.60$; unpaired t-test).
286 **h**, The released fraction of SP-pH is reduced in *Syt9* KO neurons ($n = 27$) compared to WT ($n =$
287 21) ($p = 0.0049$; Mann-Whitney test). **i**, Plot of cumulative SP-pH fusion events; again, the
288 stimulus protocol is indicated in blue. **i**, Histogram of SP-pH release event duration for WT and
289 SYT9 KO striatal neurons. **k**, Representative regions of interest (ROIs) in a timelapse,
290 demonstrating changes in SP-pH fluorescence over the course of an imaging experiment, taken
291 from **Video 1**; time points are indicated, with the stimulus at $t = 0$. The last image shows the
292 same ROI after perfusion with NH_4Cl to neutralize the luminal pH of SP-pH-bearing DCVs, as
293 indicated in (**f**). $^{**}p < 0.01$
294

295 **Application of exogenous substance P rescues the SYT9 KO mIPSC phenotype**

296 Since our data suggest that SYT9 regulates SP release (**Fig. 4**), and SP is known to
297 modulate mIPSC frequency in striatal neurons (He et al., 2019), we sought to determine
298 whether the *Syt9* KO phenotype could be rescued via acute application of this neuropeptide. In
299 addition to SP, enkephalins, dynorphins, and cholecystokinin are also enriched in the striatum
300 (Angulo & McEwen, 1994; Krause et al., 1987), so we also assayed the effects of each of these
301 neuropeptides (**Fig. 5a**). Acute addition of SP to the bath fully rescued the decreased mIPSC
302 frequency in *Syt9* KO neurons. Rescue was also observed using GR73632, a synthetic NK1R
303 agonist. In contrast, dynorphin A (DynA), Leu-enkephalin (L-Enk), and cholecystokinin (CCK8)
304 (**Fig. 5b**) had no effect, demonstrating that the mIPSC phenotype is SP-specific. Also, we found
305 that SP supplementation did not significantly change the mIPSC frequency of WT neurons,
306 indicating a high degree of SP-receptor activation under basal conditions.

307 Next, we further explored the SP-NK1R pathway using a pharmacological approach.
308 Application of SR140333, a synthetic NK1R antagonist (Jung et al., 1994), to WT neurons,
309 phenocopied the *Syt9* KO; mIPSC frequency was reduced ~2-fold (**Fig. 5b**). This finding is
310 consistent with a previous study utilizing a different NK1R antagonist (He et al., 2019), and
311 confirms that the SP-NK1R pathway serves to regulate mini frequency in striatal neurons.

312 Consistent with this model, SR140333 had no effect on mini frequency in *Syt9* KO neurons,
313 presumably due to the large reduction in SP release from these cells and the concomitant
314 decrease in NK1R activation. No differences in mIPSC amplitude were observed across all
315 conditions (**Fig. 5c**)**.** In summary, SYT9 regulates SP release, and activation of the NK1R by SP
316 is pivotal in the regulation of mIPSCs in striatal neurons.

317 The binding of SP to the NK1 receptor presumably activates $G_{q/11}$, resulting in the
318 generation of IP_3 and the mobilization of Ca^{2+} from internal stores. While basal presynaptic
319 $[Ca^{2+}]_i$ did not appear to be altered in the *Syt9* KO striatal neurons (**Supp. Fig. 7**), it has been
320 shown that local, transient increases in $[Ca^{2+}]_i$, mediated by IP_3 receptors in the presynaptic ER,
321 drive spontaneous neurotransmitter release in pyramidal neurons (Emptage et al., 2001; Simkus
322 & Stricker, 2002). We therefore speculate that decreased SP-mediated IP_3 signaling in the *Syt9*
323 KO underlies the decreased mIPSC phenotype observed in our studies.
324
325 **Figure 5**

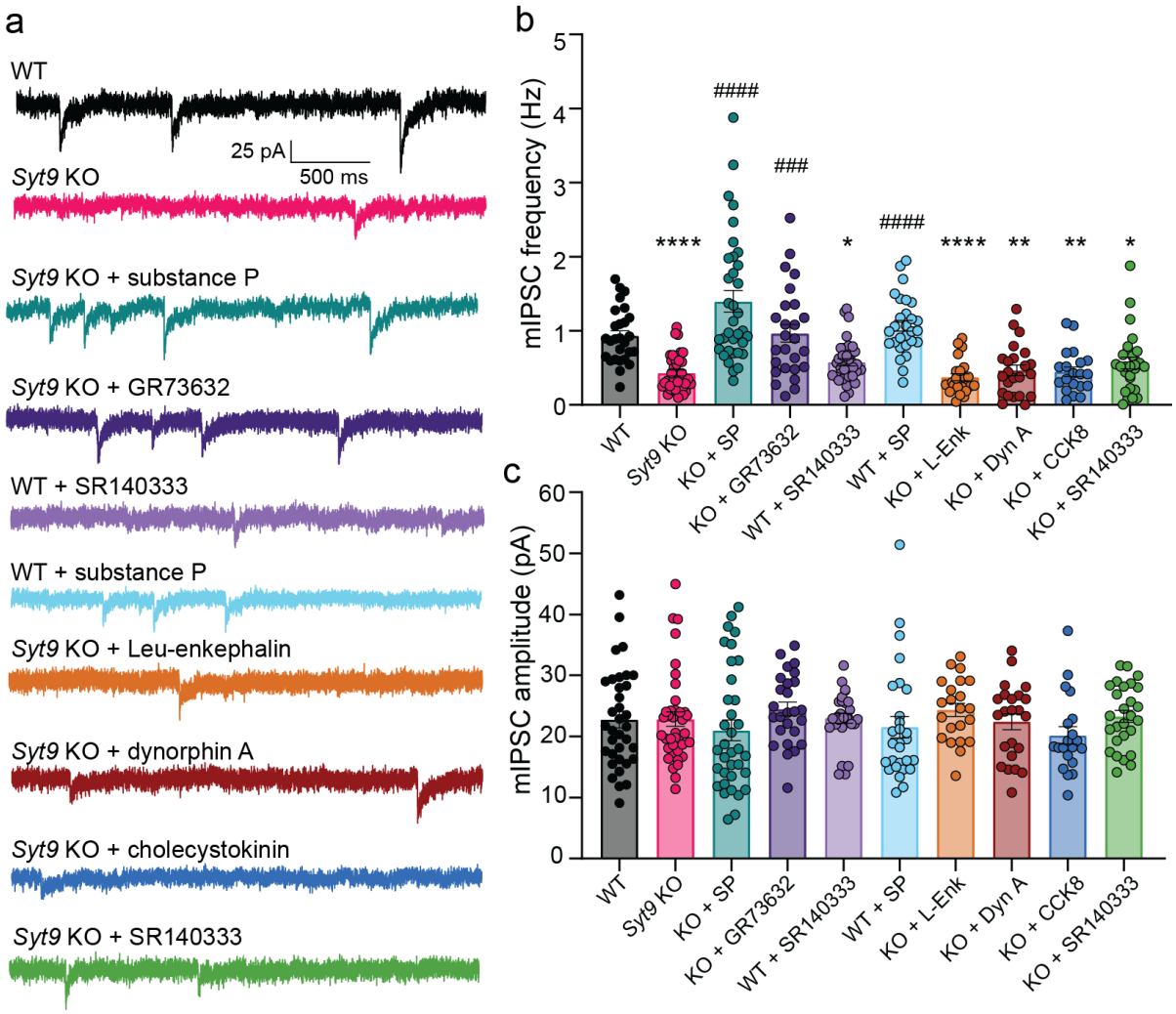

Figure 5. Treatment with substance P rescues SYT9 KO mIPSC phenotype. a, Representative mIPSC traces recorded from striatal neurons as follows: WT (n = 35); *Syt9* KO (n = 39); WT with application of 100 nM SP (n = 28) or 10 nM SR140333 (n = 34); *Syt9* KO with application of either: 100 nM SP (n = 35), 100 nM GR73632 (n = 26), 10 nM SR140333 (n=27), 100 nM Leu-enkephalin (n = 23), 100 nM dynorphin A (n = 23), or 100 nM cholecystokinin (n = 20) in the bath solution. **b-c**, Average amplitude (**b**) and frequency (**c**) of mIPSCs recorded from (**a**). Asterisks (*) indicate statistical comparisons (one-way ANOVA with Šídák's multiple comparisons test) to WT neurons; hash symbols (#) indicate statistical comparisons to *Syt9* KO neurons. *$p < 0.05$, **$p < 0.01$; ****$p < 0.0001$; ###$p < 0.001$ and ####$p < 0.0001$.

Ca^{2+}-binding to the C2A domain of SYT9 is crucial for its function *in vitro* and in neurons

The findings presented thus far suggest a model in which SYT9 regulates SP release which, in turn, modulates mini frequency. To further evaluate this model and directly determine

340 whether SYT9 serves as a Ca^{2+} sensor for SP release, we sought to identify the structural
341 elements in SYT9 that regulate membrane fusion *in vitro*, and then correlate these findings with
342 the function of SYT9 in regulating both SP release and mini frequency. For these experiments,
343 we used soluble, cytoplasmic fragments of SYT9, and for comparison, SYT1, in a 'split t-
344 SNARE' *in vitro* fusion assay (Bhalla et al., 2006) that mimics fusion of SVs with the plasma
345 membrane in cells. In this assay, SYT fragments must first fold soluble SNAP-25B onto
346 membrane-embedded syntaxin 1A (SYX1A) for fusion with synaptobrevin 2 (SYB2)-bearing
347 liposomes to occur. Consistent with a previous study (Roper et al., 2015), the cytoplasmic
348 domains (C2AB) of both SYT1 and SYT9 stimulated fusion to similar extents in the presence of
349 Ca^{2+} (omitted for clarity in **Fig. 6a** left panel but quantified in **Fig. 6a** right panel). We extended
350 these experiments by evaluating the isolated C2-domains of each isoform and found that the
351 C2A domain of SYT9 strongly stimulated fusion in response to Ca^{2+}, while C2B had little effect
352 (**Fig. 6a**). This is in sharp contrast to SYT1, where C2B, but not C2A, facilitated fusion (**Fig. 6a**)
353 (Gaffaney et al., 2008). Additionally, we utilized Ca^{2+} ligand mutants (CLMs), in which two native
354 Asp residues that serve as conserved Ca^{2+} ligands in numerous isoforms were substituted with
355 Asn, in either C2A or C2B of SYT9. These mutations disrupted the Ca^{2+} binding activity (**Fig. 6c**)
356 of each C2-domain and abolished the ability of the C2A domain of SYT9 to stimulate membrane
357 fusion in response to Ca^{2+} (**Fig. 6a**). Hence, these two related isoforms have diverged
358 unexpectedly, with C2A serving as the primary Ca^{2+} sensing domain in SYT9, while C2B is
359 more crucial in SYT1.

360 Since SYT1 regulates fusion via interactions with membranes that harbor anionic
361 phospholipids (Bai et al., 2016; Bhalla et al., 2005; Liu et al., 2014), we assayed the ability of
362 SYT9 to bind phosphatidylserine (PS)-harboring membranes in the presence and absence of
363 Ca^{2+}. A previous study reported that for SYT9 C2A, but not C2B, bound to PS-bearing vesicles
364 (Shin et al., 2004). We found that each of the isolated C2-domains efficiently bound to
365 liposomes, in response to Ca^{2+}, when the mole fraction of PS was increased from 15% to 25%;

366 this interaction is physiologically relevant since PS is ~22% of the inner leaflet of the plasma
367 membrane (Hamilton et al., 2000) (**Fig. 6b**).
368 We also directly measured Ca^{2+} binding to the isolated C2-domains of SYT9, using
369 isothermal titration calorimetry (ITC); calorimetry data for SYT1 has been previously reported
370 (Evans et al., 2016; Radhakrishnan et al., 2009). Ca^{2+} binding to SYT9 C2A was endothermic
371 and binding to C2B was exothermic (**Fig. 6c**). When fitted with a sequential binding site model,
372 C2A exhibited three binding sites with K_d values of 53 μM, 182 μM, and 337 μM; C2B had two
373 binding sites, with K_d values of 43 μM and 500 μM (see **Supplementary Table 1** for all
374 thermodynamic values). Interestingly, the K_d value for the third binding site of C2A (337 μM)
375 was significantly lower than the value reported for SYT1 (K_d > 1 mM (Evans et al., 2016;
376 Radhakrishnan et al., 2009; Ubach et al., 1998). Titrations were also performed on the CLM
377 forms of isolated C2A or C2B, described above, and these constructs yielded little to no signal,
378 confirming they fail to bind Ca^{2+} (**Fig. 6c**). These experiments demonstrate that while both
379 isolated C2-domains bind Ca^{2+}, only C2A was able to effectively stimulate membrane fusion.
380
381 **Figure 6**

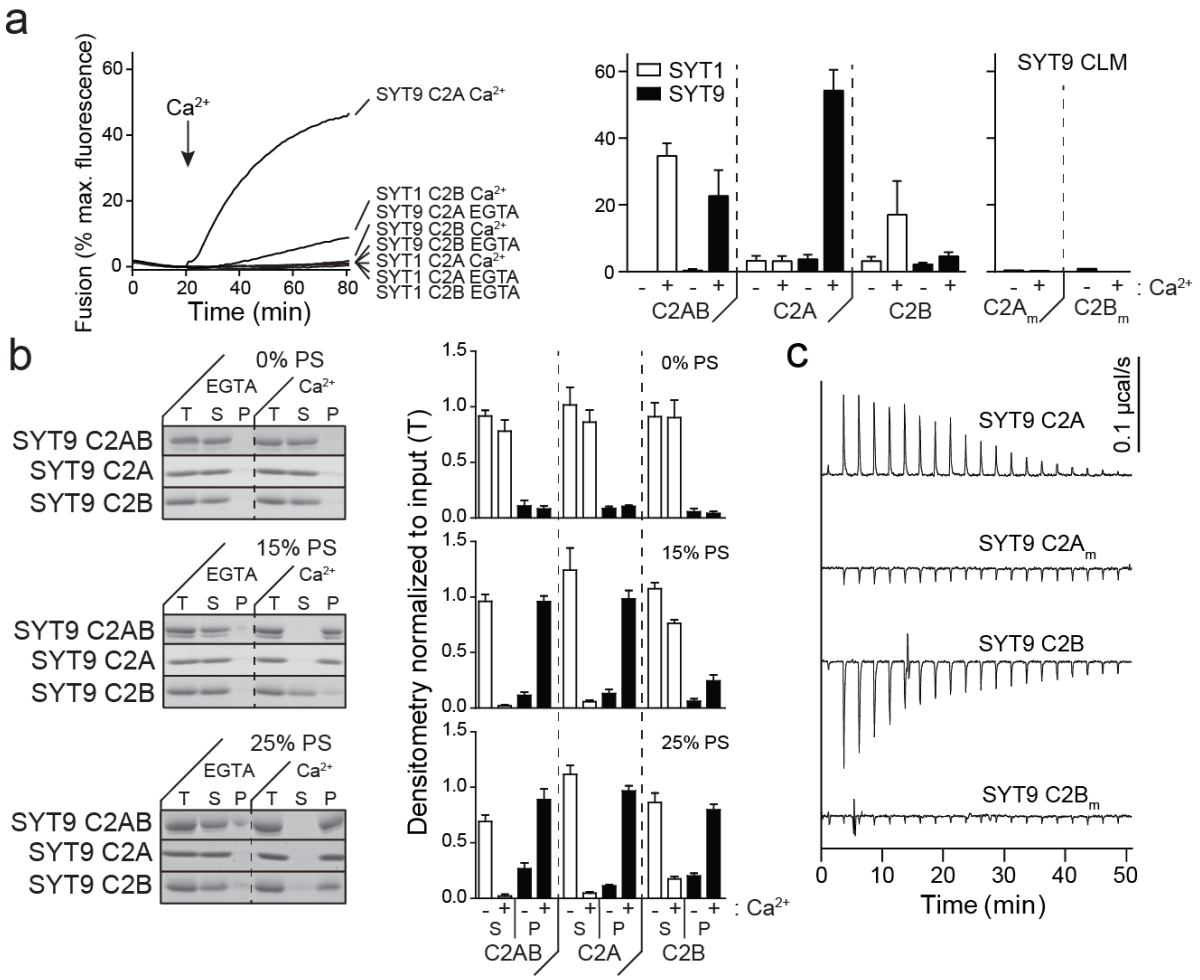

Figure 6. Ca^{2+}•C2A from SYT9 regulates membrane fusion *in vitro*. a, *Left panel:* Reconstituted split t-SNARE fusion assay where Ca^{2+}•SYT fragments must fold soluble SNAP-25B onto membrane-embedded SYX1A for fusion with SYB2 proteoliposomes to occur. Representative fusion traces, using each isolated C2-domain, C2A and C2B, from SYT1 and SYT9 are shown (left); the tandem C2-domains, C2AB, for each isoform were also assayed in parallel but were omitted for clarity. The isolated C2A domain, but not the C2B domain, of SYT9 stimulated fusion; in SYT1, C2B, rather than C2A, stimulated fusion (Gaffaney et al., 2008). *Right panel*: The extent of fusion (80 min), using all SYT constructs, in the presence (+) or absence (-) of Ca^{2+}, is plotted (n ≥ 3). **b**, Binding of SYT9 C2A, C2B, and C2AB to PS-bearing liposomes was monitored via a co-sedimentation assay. Representative SDS-PAGE gels of protein from equal fractions of the supernatant (S), and pellet (P), as well as the total input (T), in the absence (0.2 mM EGTA) or presence of Ca^{2+} (1 mM free), using liposomes with 0, 15 and 25% PS, are shown (left). Protein band intensities were normalized to the total input and plotted (right; n ≥ 3). **c**, Representative ITC traces showing the heat of Ca^{2+} binding to the isolated C2-domains of WT SYT9; the Ca^{2+} ligand mutant (CLM) domains were analyzed in parallel, confirming that they fail to bind Ca^{2+} (n = 4). Thermodynamic values are provided in **Supplementary Table 1**.

401 Next, if our model is correct, the biochemical results above suggest that Ca^{2+} binding to
402 C2A, but not C2B, should underlie the ability of SYT9 to promote SP release. To test this, full-
403 length variants of the SYT9 CLMs were generated and expressed in SYT9 KO neurons via
404 lentiviral transduction; WT SYT9 served as a positive control. SP release was monitored using
405 the optical assay described in **Figure 4**. Importantly, $C2A_mB$ and $C2A_mB_m$ failed to rescue
406 release, while $C2AB_m$ exhibited full rescue (**Fig. 7a**) with no change in DCV pool size (**Fig. 7b**).
407 Hence, the ability of these mutants to regulate reconstituted membrane fusion reactions *in vitro*,
408 and to drive SP release from living neurons, were well correlated; in both cases, the C2A
409 domain functioned as the crucial Ca^{2+}-sensing motif. These findings further support the idea that
410 SYT9 functions as a Ca^{2+} sensor for DCV exocytosis.
411 Finally, we conducted patch-clamp recordings of *Syt9* KO striatal neurons that
412 expressed each full-length CLM construct. Again, complete rescue of mIPSC frequency was
413 observed using WT SYT9. In sharp contrast, SYT9 $C2A_mB_m$, which cannot bind Ca^{2+} via either
414 C2-domain, failed to rescue the mini phenotype. Consistent with our model, $C2A_mB$ also failed
415 to rescue (**Fig. 7c**), while $C2AB_m$ was as effective as the WT protein (**Fig. 7d**; note: no changes
416 in mini amplitude were observed across conditions [**Supp. Fig. 8**]). In summary, Ca^{2+} binding to
417 the C2A domain, but not the C2B domain, underlies the ability of SYT9 to regulate membrane
418 fusion to, in turn, indirectly control the rate of spontaneous release in striatal neurons by
419 controlling SP secretion.
420
421 **Figure 7**

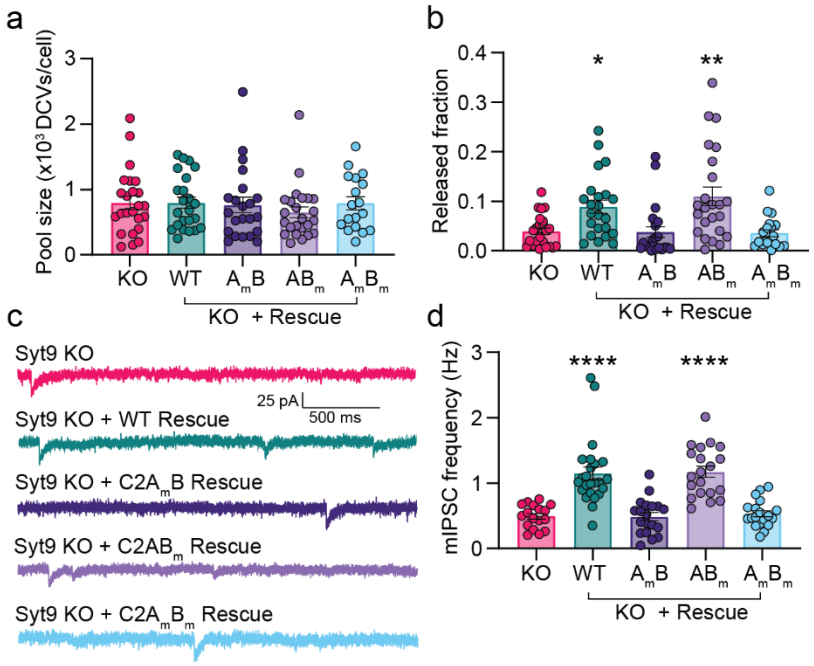

Figure 7. The Ca^{2+}-binding activity of the C2A domain of SYT9 is required for its action in neurons. a, SP-containing DCV pool size was unchanged across *Syt9* KO rescue conditions (p = 0. 6272; Kruskal-Wallis test). **b**, The reduction in SP-pH release in *Syt9* KO striatal neurons (n = 21) was rescued by expression of WT SYT9 (n = 23) (p = 0.0158) or the C2AB$_m$ mutant (n = 24) (p = 0.0069). In contrast, the C2A$_m$B (n = 22) (p > 0.9999) and C2A$_m$B$_m$ mutants (n = 19) (p > 0.9999) both failed to rescue release. Release was monitored as shown in (**Fig. 4e-k**). **c**, Representative mIPSC traces recorded from striatal neurons as follows: *Syt9* KO (n = 17), *Syt9* KO + WT rescue (n = 24), *Syt9* KO + C2A$_m$B rescue (n = 19), *Syt9* KO + C2AB$_m$ rescue (n = 20), and *Syt9* KO + C2A$_m$B$_m$ (n = 19) rescue. **d**, Average frequency of mIPSCs recorded from (**c**). WT SYT9 and C2AB$_m$ mutant rescued the mini frequency, while the C2A$_m$ and C2A$_m$B$_m$ mutants failed to rescue this phenotype. In this figure, asterisks (*) indicate statistical comparisons (Kruskal-Wallis test with Dunn's multiple comparisons test) to the *Syt9* KO condition.

DISCUSSION

SYT9 is widely expressed in the brain ([Mittelsteadt et al., 2009]; note: these authors referred to SYT9 as SYT5), but KOs lacking this protein have only been characterized using the calyx of Held slice preparation (Kochubey et al., 2016) and cultured striatal neurons (Xu et al., 2007). SYT9 appears to be expressed in the calyx of Held, but loss of this protein did not affect AP-triggered neurotransmitter release (Kochubey et al., 2016). In contrast, in cultured striatal

443 neurons, Xu et al. (2007) reported a 57% reduction in eIPSC amplitude in *Syt9* KO striatal
444 neurons. However, this finding has not been reproduced, and it is difficult to reconcile with the
445 expression patterns of SYT9 and SYT1. Namely, SYT9 is expressed at similar levels in cortical,
446 hippocampal, and striatal neurons, and it is well-established that loss of SYT1 abolishes
447 synchronous release in both cortical and hippocampal neurons (Geppert et al., 1994; Maximov
448 & Südhof, 2005) (**Fig 1**). So, it is apparent that endogenous SYT9 does not function as a Ca^{2+}
449 sensor for synchronous SV exocytosis in either of these two classes of neurons (**Fig. 1; Supp.**
450 **Fig. 1**). Here, we extended these observations to cultured striatal neurons and found that SYT1,
451 but not endogenous SYT9, drives rapid SV exocytosis. We went on to show that SYT9 is largely
452 localized to SP-bearing DCVs in striatal neurons, where it regulates the release of this
453 neuropeptide to indirectly control mIPSC frequency. Evidently, at least some isoforms of SYT
454 have become specialized to control the release of neuropeptides that impact synaptic function
455 (Cao et al., 2011; Dean et al., 2009; Dean, Liu, et al., 2012). It is tempting to speculate the
456 divergence of numerous SYT isoforms might enable the differential release of myriad distinct
457 neuromodulators and hormones, in response to different patterns of activity.
458 We found that SYT9 is expressed at ~25-fold lower levels than SYT1 (**Fig. 1**). Given the
459 estimate of ~15 copies of SYT1 per SV (Takamori et al., 2006), the abundance of SYT9 on SVs
460 would, on average, be expected to be low, particularly since its primary localization appears to
461 be on DCVs (**Fig. 4**). Some fraction of SYT9 does colocalize with canonical SV markers (**Fig. 2**;
462 (Xu et al., 2007), and SYT9 was detected in proteomic studies of purified SVs ([Takamori et al.,
463 2006; Taoufiq et al., 2020] note: these authors referred to SYT9 as SYT5). Thus, it remains
464 possible that there could be limited populations of SVs, in discrete brain regions, which harbor a
465 sufficient copy number of SYT9 molecules to trigger SV exocytosis. However, in our hands, this
466 was not the case with cortical, hippocampal, or striatal neurons (**Fig 1; Supp. Fig. 1**). It should
467 also be emphasized that DCVs are often present in or near presynaptic nerve terminals

468 (Persoon et al., 2018; Radhakrishnan et al., 2021), and this can potentially exaggerate the
469 presence of SYT9 on SVs as determined via immunocytochemistry.

470 While our experiments indicate that SYT9 functions as a Ca^{2+} sensor for SP release
471 from striatal neurons, some degree of regulated release persisted in the KO (**Fig. 4**), suggesting
472 that additional Ca^{2+} sensors are associated with SP-bearing DCVs. Indeed, SYT1 was present
473 on SP-bearing DCVs purified from rabbit optic nerve (Berg et al., 2000). Additionally, in
474 hippocampal neurons, SYT1 and SYT7 have both been implicated in DCV exocytosis (van
475 Westen et al., 2021), suggesting multiple roles for these Ca^{2+} sensors. We also note that SYT4,
476 which does not bind Ca^{2+}, negatively regulates the release of brain-derived neurotrophic factor
477 (BDNF) (Dean et al., 2009), and SYT10, which binds Ca^{2+}, positively regulates the secretion of
478 IGF-1 from DCVs in neurons (Cao et al., 2011). Collectively, these findings, combined with the
479 observations in the current study, support the idea that the SYTs have diverged, at least in part,
480 to control different forms of DCV exocytosis (Dean, Dunning, et al., 2012). We also reiterate that
481 the *Syt9* KO mIPSC phenotype appears to be specific for striatal neurons, which robustly
482 express SP. The function of SYT9 in cortical and hippocampal neurons remains unknown. We
483 speculate that it regulates the release of neuropeptides; a future goal is to address this issue via
484 co-localization studies and by isolating and characterizing SYT9-bearing organelles from these
485 classes of neurons.

486 Regarding the diversity of SYT isoforms, our finding that the C2A domain of SYT9
487 serves as the crucial Ca^{2+}-sensing motif for fusion was unexpected. SYT9 forms a clade with
488 SYT1/2, and Ca^{2+} ligand mutations in the C2B-domain of SYT1 clearly disrupt function (Nishiki
489 & Augustine, 2004), while similar mutations in C2A have been reported to either have no effect
490 (Fernández-Chacón et al., 2002), to be gain-of-function (Pang, Shin, et al., 2006; Stevens &
491 Sullivan, 2003), or to cause partial loss-of-function (Shin et al., 2009). Moreover, the isolated
492 C2B domain of SYT1, but not the C2A domain, regulates fusion *in vitro* (**Fig. 6**; (Gaffaney et al.,
493 2008). In contrast, Ca^{2+}-binding to the C2A domain of SYT9, but not the C2B domain, was

494 required to both stimulate fusion *in vitro* (**Fig. 6**) and promote SP release from striatal neurons
495 (**Fig. 7a,b**), to regulate minis (**Fig. 7c,d**). Apparently, this shuffling of C2-domain function is
496 tolerated, as SYT9 can rescue evoked neurotransmitter release and clamp spontaneous release
497 in *Syt1* KO neurons, when sufficiently over-expressed (**Fig. 2**).

498 Returning to the physiology, we emphasize that the striatum is a specialized structure
499 with a dense local network largely composed of medium spiny neurons (MSNs) and their axon
500 collaterals. While a substantial fraction of these neurons projects to other brain regions, direct
501 synaptic communication between MSNs also occurs (Koos et al., 2004; Tunstall et al., 2002);
502 this is the condition recapitulated in our experiments using cultured striatal neurons.
503 Subpopulations of MSNs release SP within the striatum (Gerfen, 1992) and harbor NK1
504 receptors (Almeida et al., 2004; Haneda et al., 2007). We observed modulation of MSN-MSN
505 transmission by SP in culture, and the next step will be to measure such modulation in acute
506 striatal slice preparations. In addition, MSNs project to targets in the substantia nigra and globus
507 pallidus, and recordings from brain slices that encompass the striatum along with these other
508 structures will address the role of SYT9-regulated SP release at terminals that innervate these
509 target cells. Moreover, SP enhances center-surround contrast of striosomal dopamine signals
510 by modulating dopamine release from neurons that project from the substantial nigra onto
511 striatal targets (Brimblecombe & Cragg, 2015). Hence, slice recordings, to measure dopamine
512 release, are an important future direction of this work.

513 We propose that SP modulates spontaneous release rates in striatal neurons by binding
514 the NK1 receptor and activating $G_{q/11}$, resulting in the generation of IP_3 and the mobilization of
515 Ca^{2+} from internal stores (**Fig. 8**), thus increasing mini frequency. Indeed, localized increases in
516 $[Ca^{2+}]_i$, mediated by IP_3 receptors in the presynaptic ER, have been reported to drive
517 spontaneous release in pyramidal neurons (Emptage et al., 2001; Simkus & Stricker, 2002). A
518 future goal is to compare these brief Ca^{2+} transients, akin to Ca^{2+} sparks in muscle cells, in WT
519 and *Syt9* KO striatal neurons. Finally, we emphasize that the highest expression levels of SYT9

520 in mouse brain occur in the pituitary gland and hypothalamus, both of which are particularly rich
521 sources of numerous classes of DCVs (Roper et al., 2015). It will be interesting to investigate
522 whether SYT9 regulates the release of hypothalamic hormones.
523
524 **Figure 8**

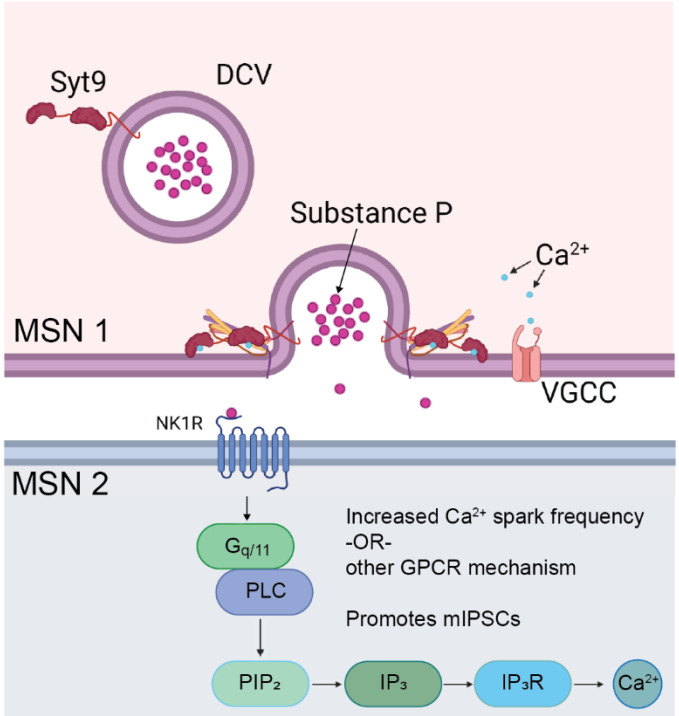

525

526 **Figure 8. SYT9 indirectly controls mini frequency in striatal neurons by serving as a Ca^{2+}**
527 **sensor for SP exocytosis.** A model in which SYT9 serves as a Ca^{2+} sensor that regulates the
528 exocytosis of SP-containing DCVs from striatal neurons. Released SP then activates the NK1
529 receptor which in turn activates the IP_3 pathway via $G_{q/11}$ and phospholipase C (PLC), leading to
530 increased Ca^{2+} efflux from the ER, to promote spontaneous neurotransmitter release rates.
531

532 **MATERIALS AND METHODS**

533

534 **Animals**

535 All neuronal cultures were prepared from early postnatal (P0-P1) mice in accordance
536 with all relevant regulations and the approval of the University of Wisconsin Institutional Animal
537 Care and Use Committee. Conditional *Syt9 KO* mice were obtained from Jackson Labs (Xu et

538 al. 2007). These conditional *Syt9* KO mice were terminally crossed with an E2a-CRE mouse
539 (Jackson Labs, Bar Harbor, ME, USA) to yield a population of constitutive *Syt9* KO mice; the
540 mice used in this study are all products of this constitutive *Syt9* KO mouse. *Syt1* cKO
541 (conditional KO) mice were a gift from W. Thoreson, (University of Nebraska-Lincoln, Lincoln,
542 NE, USA; [Quadros et al., 2017]).
543
544 **Genotyping**
545 The *Syt9* KO mouse line was maintained as heterozygous breeders so that offspring WT
546 and KO littermates could be studied. To genotype the neonatal pups, tissue samples were taken
547 by collecting ~2 mm of the end of the tail and extracting DNA from the tissue sample using the
548 Kapa Express Extract Kit (Kapa Biosystems, Wilmington, MA, USA). The extracted DNA was
549 then subjected to PCR using in-house designed primers to identify WT and KO alleles. The
550 primers used to identify the WT allele yield a 209 bp amplicon: F-primer 5'-
551 GCGTCAATGGGAGGAGAGGTCA-3'; R-primer 5'-GTCCACTAGGGCTAGCCCAGG-3'. The
552 primers used to identify the KO allele yield a 301 bp amplicon: F-primer 5'-
553 CAGTAGGGAGCGAGCAGAAATTAAAAT-3'; R-primer 5'-
554 AACTTCGTCGATCGACCTCGAATAA-3'. The PCR product was subjected to agarose gel
555 electrophoresis and imaged on a ChemiDoc MP imaging system (BioRad, Hercules, CA, USA).
556
557 **Molecular biology and lentiviral preparation**
558 Lentiviral vectors were based on FUGW (FUGW was a gift from David Baltimore
559 [Addgene plasmid # 14883; http://n2t.net/addgene:14883; RRID: Addgene_14883]) (Lois et al.,
560 2002). The FUGW vector was modified by substituting the ubiquitin promoter with the human
561 synapsin I promoter (Kügler et al., 2003); this vector is henceforth referred to as FSGW. pH-
562 SYT9 was generated by replacing SYT1 in pHluorin-SYT1 (a gift from J. Rothman, Yale
563 University, New Haven, CT) (Fernández-Alfonso et al., 2006) with a SYT9 cDNA (a gift from M.

564 Fukuda, Tohoku University, Sendai, Miyagi, Japan) (Haberman et al., 2003) using PCR splicing
565 via overlap extension (SOE). The pHluorin-SYT9 cassette replaced GFP in the cloning site of
566 the FSGW vector via In-Fusion Cloning (Takara Bio, San Jose, CA, USA). The SP-pH construct
567 was generated by PCR SOE and comprised: the first 68 residues of mouse preprotachykinin
568 (PPT), a GS$(GSS)_4$ linker, and a super-ecliptic pHluorin (Miesenböck et al., 1998). This fusion
569 construct was subcloned into FSGW.

570 SYT9 CLM constructs correspond to D-to-N substitutions of two Ca^{2+} ligands in each C2-
571 domain as follows: $C2A_mB$; D197N and D199N; $C2AB_m$; D330N and D332N. All four mutations
572 are present in the $C2A_mB_m$ construct. These constructs were made by performing site-directed
573 mutagenesis on the *Syt9* cDNA with the QuikChange Lightning Site-Directed Mutagenesis Kit
574 (Agilent, Santa Clara, CA, USA). Full-length CLM constructs were used for the rescue
575 experiments in Fig. 7, and isolated purified C2-domain CLM constructs were used for Fig. 6.
576 cDNA for SNAP-25B was provided by M. C. Wilson (University of New Mexico School of
577 Medicine, Albuquerque, NM, USA), and full-length synaptobrevin 2 (SYB2) and syntaxin 1A
578 (SYX) were provided by J. Rothman (Yale University, New Haven, CT); these SNARE proteins
579 were subcloned into pTrcHis vectors to yield His_6-tagged proteins (Evans et al., 2015).
580

581 **Cell culture, transient transfection, and lentiviral transduction**

582 Cortical, hippocampal, and striatal regions were obtained by microdissection and kept in
583 ice-cold Hibernate-A (BrainBits, Springfield, IL, USA) with 2% B-27 until completion of
584 dissection. Neural tissue was then incubated with 0.25% trypsin-EDTA (Corning Inc., Corning,
585 NY, USA) for 25 minutes at 37°C. The tissue was washed with DMEM (Gibco, Carlsbad, CA,
586 USA) supplemented with FBS (Atlanta Biologicals, Flowery Branch, GA, USA) and penicillin-
587 streptomycin (Thermo Scientific, Waltham, MA, USA) and triturated 10-15 times with a P1000
588 pipette tip until complete dissociation of the tissue. Cells were plated at a density of 100,000
589 cells/cm^2 onto poly D-lysine-coated glass coverslips. Supplemented DMEM was replaced after 1

590 hour with Neurobasal-A (Gibco) supplemented with B-27 (Thermo Scientific) and GlutaMAX
591 (Thermo Scientific). For SP-pH release experiments, sparse transfection of SP-pH and a
592 cytosolic mRuby marker was required for identifying and imaging single neurons. This was
593 achieved using Lipofectamine LTX with PLUS reagent (Invitrogen, Carlsbad, CA, USA) on DIV
594 8-9. For localization studies, rescue experiments, and Ca^{2+} imaging, full coverage was desirable
595 and was achieved via lentiviral transduction. Lentivirus encoding CRE-recombinase was added
596 to *Syt1* cKO neurons at DIV 0-2, and lentiviruses that expressed SYT9 rescue constructs, the
597 Ca^{2+} imaging construct synaptophysin-HaloTag (SYP-Halo) (Bradberry & Chapman, 2022), or
598 SP-pH for localization studies, were added to neurons at DIV 5-7.
599
600 **Electrophysiological studies**
601 Whole-cell voltage-clamp recordings of cultured neurons (DIV 14-18) were performed at
602 room temperature in artificial cerebrospinal fluid (ACSF) containing (in mM): 128 NaCl, 5 KCl,
603 1.5 $CaCl_2$, 1 $MgCl_2$, 30 glucose, 25 HEPES, pH 7.4 with an internal solution containing (in mM):
604 130 KCl, 10 HEPES, pH 7.4, 1 EGTA, 2 ATP, 0.3 GTP, 5 phosphocreatine. Recordings were
605 performed using a MultiClamp 700B amplifier and Digidata 1550B digitizer (Molecular Devices,
606 San Jose, CA, USA) under the control of Clampex 10 software (Molecular Devices). $GABA_A$-
607 mediated currents were pharmacologically isolated using 20 μM CNQX (Tocris Bioscience,
608 Bristol, UK) and 50 μM D-AP5 (Tocris) in the bath solution; for mIPSC recordings, 1 μM
609 tetrodotoxin (Tocris) was included in the bath. 5 mM QX 314 chloride (Tocris) was included in
610 the pipette solutions for all recordings. Neurons were held at -70 mV in all experiments without
611 correction for liquid junction potentials. Recordings were discarded if series resistance rose
612 above 15 MΩ. For evoked recordings, a concentric bipolar electrode (FHC, Bowdoin, ME, USA)
613 was placed 100-200 μm away from the patched soma and stimulation currents were adjusted to
614 evoke maximal responses. For mIPSC recordings, 300 s of data were recorded for each striatal
615 neuron, and 180 s of data were acquired for cortical and hippocampal neurons. mIPSCs were

616 quantified for each recording using a template-matching algorithm in Clampfit (Molecular
617 Devices). For pharmacology rescue experiments, SP (Tocris), GR73632 (Tocris), Leu-
618 enkephalin (Tocris), dynorphin A (Tocris), and cholecystokinin (Tocris) were added to the ACSF
619 at 100 nM, except for SR140333 (Tocris), which was added at 10 nM. Neurons were treated
620 with peptides or drugs for ten minutes before patch-clamp experiments were conducted.
621
622 **Immunoblotting**
623 Coverslips of cultured neurons (DIV 14-18) were rinsed 1-2 times in PBS and lysed by
624 repeated pipetting of lysis buffer (50 mM Tris pH 8.0, 150 mM NaCl, 2% SDS, 0.1% Triton X-
625 100, 10 mM EDTA) containing a protease inhibitor cocktail (cOmplete mini EDTA-free, Roche).
626 For quantitative Western blots of lysates, protein concentration was determined using a
627 bicinchoninic acid (BCA) assay (Thermo Scientific) to ensure equal amounts of protein were
628 subjected to SDS-PAGE. Samples were then combined with 4x Laemmli sample buffer, heated
629 to 50°C for 15 minutes, and stored at -20°C until use. For each immunoblot experiment, the
630 samples were subjected to SDS-PAGE on 13% polyacrylamide gels containing 1%
631 trichloroethanol (TCE). After electrophoresis, the TCE was activated by exposure to UV light
632 (300 nm) for 45 seconds, and labeled proteins were detected via 300 nm illumination; these
633 signals served as a protein loading control (Ladner et al., 2004). Proteins were transferred to a
634 PVDF membrane, which was then blocked with 5% nonfat milk in Tris-buffered saline plus 0.1%
635 Tween 20 (TBST) for 1 hour, followed by incubation with primary antibody overnight at 4°C.
636 Blots were then washed 3 times for 5 minutes in TBST, incubated with secondary antibody for 1
637 hour, and washed again as above. For the pH-SYT9 rescue experiments, after blotting for
638 SYT9, the PVDF membranes were stripped using Restore™ Western Blot Stripping Buffer
639 (Thermo Scientific), and the membranes were once again blocked and subsequently probed for
640 SYT1. Primary antibodies were: α-SYT1 (1:500) (DSHB; #mAB 48; RRID:AB_2199314) and α-
641 SYT9 (1:500) (Synaptic Systems Cat# 105 053, RRID:AB_2199639). Secondary antibodies

642 were goat α-mouse IgG-HRP (Biorad, 1706516; RRID:AB_11125547), goat α-mouse IgG2b-
643 HRP (Invitrogen, M32407; RRID:AB_2536647), and goat α-rabbit IgG-HRP (Biorad, 1706515,
644 RRID:AB_11125142). Immunoreactive bands were visualized using SuperSignal West Pico
645 Plus Chemiluminescent Substrate (Thermo Scientific) and imaged with an Amersham Imager
646 680 imaging system (GE Healthcare, Chicago, IL, USA). Bands were analyzed by densitometry,
647 with care to stay within the linear range, and contrast was linearly adjusted for publication using
648 ImageJ (Fiji) (Schindelin et al., 2012).
649
650 **Immunocytochemistry and confocal microscopy**
651 Immunocytochemistry was conducted as previously described (Courtney et al., 2019).
652 For the pH-SYT9 rescue experiments, immediately before fixation and permeabilization, cortical
653 neurons were incubated in primary antibody directed against the pHluorin tag of pH-SYT9
654 (1:250) (α-GFP; Abcam Cat# ab290, RRID: AB_303395) in culture medium to label only the
655 surface-resident pH-SYT9, as the antibody is unable to enter intact, live neurons. Unbound
656 antibody was removed by washing, and then cells were fixed and permeabilized and incubated
657 a second time with primary antibodies to label synaptophysin (1:1000) (α-SYP; Synaptic
658 Systems Cat# 101 004; RRID:AB_1210382) and pHluorin (1:1000) (α-GFP; Abcam Cat#
659 ab13970, RRID:AB_300798). This second α-GFP antibody labeled all pHluorin tags that were
660 not labeled by the first α-GFP 'blocking' antibody, to reveal the internal fraction of pH-SYT9.
661 This strategy allowed for differential secondary labeling of the different pH-SYT9 populations
662 with species-specific secondary antibodies.
663 Images were acquired on a Zeiss LSM 880 laser scanning confocal microscope with a
664 63x Plan-Apochromat 1.4NA DIC oil immersion objective. Identical laser and gain settings were
665 used for all samples within each experimental paradigm. Primary antibodies were: α-GFP
666 (1:1000) (Abcam Cat# ab290, RRID:AB_303395), α-GFP (1:1000) (Abcam Cat# ab13970,
667 RRID:AB_300798), α-SYT1 (1:500) (DSHB; #mAB 48; RRID:AB_2199314), α-SYP (1:1000)

668 (Synaptic Systems Cat# 101 004; RRID:AB_1210382), α-SYT9 (1:500) (Synaptic Systems Cat#
669 105 053, RRID:AB_2199639), α-CHGB (Synaptic Systems Cat# 259 103; RRID:AB_2619973),
670 α-VGAT (1:1000)(Synaptic Systems Cat # 131 004; RRID:AB_887873), α-Gephyrin
671 (1:1000)(OriGene Cat# TA502313, RRID:AB_11126039), and α-MAP2 (1:500) (Abcam Cat#
672 ab5392, RRID:AB_2138153). Secondary antibodies were: goat anti-chicken IgY-Alexa Fluor
673 405 (1:500) (abcam; ab175675, RRID:AB_2810980), goat α-chicken IgY-Alexa Fluor 488
674 (1:500) (Thermofisher A-11039, RRID: AB_2534096), goat α-guinea pig IgG-Alexa Fluor 488
675 (1:500) (Thermofisher; A-11073; RRID:AB_2534117), goat α-rabbit IgG-Alexa Fluor 546 (1:500)
676 (Thermofisher; A-11010, RRID:AB_2534077), goat α-guinea pig IgG-Alexa Fluor 647 (1:500)
677 (Thermofisher; A-11074, RRID:AB_2534118), and goat α-mouse IgG2b-Alexa Fluor 647 (1:500)
678 (Thermofisher; A-21242; RRID:AB_2535811).
679
680 **Live cell imaging**
681 DIV 14-18 striatal neurons were washed twice in ASCF before being mounted in an
682 imaging chamber with parallel platinum electrodes (Warner Instruments, Hamden, CT, USA)
683 with 500 µL of ACSF. Imaging was carried out with a 40x, 1.4 NA oil-immersion objective on an
684 inverted epifluorescence microscope (IX81, Olympus, Tokyo, Japan) equipped with a CMOS
685 camera (Orca Flash 4.0 V2, Hamamatsu Photonics, Hamamatsu, Japan), motorized stage (Mad
686 City Labs, Madison, WI, USA), and a custom illumination source containing three LEDs (470,
687 530, 625 nm) (Thorlabs, Newton, NJ, USA). The system was controlled using Micro-Manager
688 (Edelsteinet al. 2010). Stimulation was delivered with a stimulation box (SD9, Grass Instrument
689 Co., West Warwick, RI, USA) controlled via a HEKA EPC10 DAQ-amplifier and PatchMaster
690 software (HEKA, Holliston, MA, USA), which was also used to synchronize the start of image
691 sequence acquisition. Images were collected using 2 x 2 binning (0.365 µm x 0.365 µm pixel
692 size).

693 For SP-pH release imaging, an exposure time of 100 ms was used. Individual
694 transfected neurons were identified for imaging by first detecting the cytosolic mRuby signal with
695 the 530 nm LED and standard RFP filter set (49004, Chroma, Bellows Falls, VT, USA). SP-pH
696 release was imaged with the 470 nm LED, a standard green fluorescent protein (GFP) filter set
697 (49002, Chroma). Ten seconds of baseline were obtained before stimulation was given 16
698 periods of 50 APs at 50 Hz with 0.5 sec between each train. Seventy seconds after the start of
699 stimulation, 500 µL of 2x NH_4Cl ACSF, containing (in mM): 100 NH_4Cl, 28 NaCl, 5 KCl, 1.5
700 $CaCl_2$, 1 $MgCl_2$, 30 glucose, 25 HEPES, pH 7.4, was added to dequench pHluorin fluorescence
701 to visualize the total number of SP-pH-bearing vesicles.
702 For Ca^{2+}-imaging, the 625 nm LED, custom three-band pass dichroic mirror (Chroma)
703 and far-red emission filter, and a 10 ms exposure time were used. DIV 14-18 striatal neurons
704 that were transduced with a virus that induced expression of SYP-Halo were first washed twice
705 in ACSF before being incubated in ACSF containing 100 nM of the acetoxymethyl ester of JF_{646}-
706 BAPTA bearing a HaloTag ligand (JF_{646}-BAPTA-AM-HTL)(Deo et al., 2019), a gift from L. Lavis
707 (Janelia Research Campus, Ashburn, VA, USA). After a 20-minute incubation at 37°C, the cells
708 were again washed with dye-free ACSF and incubated for 20 minutes at 37°C before being
709 mounted in the imaging chamber. Five fields of view (FOV) were selected per coverslip. Three
710 seconds of baseline were recorded before a saturating stimulus (50 AP @ 50Hz) was delivered
711 to establish a maximum fluorescence (F_{max}) for each field of view. At least five minutes elapsed
712 between imaging each FOV to give the neurons time to recover and return to basal conditions.
713

714 **Image analysis**

715 For colocalization analysis, the Coloc2 plugin in Fiji (Schindelin et al., 2012)was used to
716 determine the Mander's overlap coefficients and Pearson's correlation coefficients; Costes'
717 automatic threshold regression was used for both determinations.

718 For synapse counting analysis, images were exported to SynD (Schmitz et al., 2011),
719 where the image of MAP2 staining was used to create a neurite mask, then synaptic density
720 was quantified by counting the number of overlapping VGAT and Gephyrin puncta within the
721 neurite mask and dividing the total number by the length of dendrite measured to yield number
722 of synapses per micron.
723 For SP-pH release analysis, Fiji with the DCV_pHluorin toolset
724 (https://github.com/alemoro/DCVpHluorin_toolseet) (Moro et al., 2021) was used; 3 pixels x 3
725 pixels regions of interest (ROIs) were placed over each observed increase in fluorescence, and
726 somatic events were excluded. Fusion events were defined as a sudden increase of 2 SD
727 above the average fluorescence of the first 100 frames in the ROI (F_0). Time lapses were also
728 manually scored along with the DCV_pHluorin analysis algorithm to ensure a thorough and
729 complete characterization of each release event. Pool size estimations were calculated using
730 the same rules used for fusion event detection, after perfusion with NH_4Cl. Analysis was
731 blinded, and the number of fusion events, SP-pH vesicle pool size estimation, event duration,
732 and fusion onset timing were all determined using DCV_pHluorin. Output data were processed
733 in Excel and plotted using GraphPad Prism.
734 Ca^{2+}-imaging analysis was performed as previously described (Bradberry & Chapman,
735 2022) with a modified ImageJ script taken from (Vevea & Chapman, 2020). Briefly, SYP-
736 HaloTag-JF_{646}-BAPTA traces were background subtracted, and ROIs were created based on a
737 custom workflow to identify changes in fluorescence of the selected image series. An average
738 intensity projection of pre-stimulus baseline frames was subtracted from a maximum intensity
739 projection of the entire timelapse. This result was duplicated and mean filtered using a rolling
740 ball radius of 10 pixels. The mean filtered image was subtracted from the original result, and this
741 result was used to threshold changes in fluorescence. After thresholding, images were made
742 binary, and a watershed function was run to separate overlapping objects. Using this procedure,
743 objects (>10 pixels) were created and defined as ROIs. These ROIs were used to measure

744 fluorescence changes over time from the original image series. The fluorescence traces of each
745 ROI were then imported into AxoGraph where the basal, pre-stimulation fluorescence of each
746 ROI (F_r) was subtracted from the max fluorescence at indicator saturation (F_{max}) to give a ΔF.
747 The following equation was used to calculate presynaptic basal $[Ca^{2+}]_i$:

748 $$[Ca^{2+}]_i = K_d \left(\frac{F_r/F_{max} - 1/R_f}{1 - F_r/F_{max}}\right)$$

749 where K_d is the dissociation constant of the indicator, F_r is the baseline fluorescence of an ROI
750 pre-stimulation, F_{max} is the fluorescence achieved with the delivery of a saturating stimulus, R_f is
751 the dynamic range of the indicator, and n is the Hill coefficient. For K_d, R_f and n, we used *in vitro*
752 measurements (K_d = 140 nM, R_f = 5.5, n = 1) from (Deo et al., 2019).
753 Trafficking analysis was conducted using the Multi Kymograph plugin in Fiji; 30-second
754 time-lapses, taken after NH_4Cl perfusion in the SP-pH release experiments, were used. Ninety
755 μm segments that began within 20 μm of the soma were chosen. The kymograph was created
756 from this time-lapse and every path was traced and quantified.
757
758 **Protein Purification**
759 Recombinant proteins were made as described (Evans et al., 2015). SYB2, SNAP-25B,
760 and SYX were purified as His_6-tagged proteins using the pTrcHis vector. The SYT1 cytoplasmic
761 domain (SYT1 C2AB – residues 96-421; the amino acid residues of the other SYT constructs
762 are indicated in parentheses), SYT1 C2A (96-264), and SYT1 C2B (248-421), were purified as
763 GST-tagged proteins using a pGEX vector. The SYT9 cytoplasmic domain (SYT9 C2AB –104-
764 386), SYT9 C2A (124-211), and SYT9 C2B (253-344) were purified as His_6-tagged proteins
765 using the pTrcHis vector. Isolated SYT9 C2A and C2B domains, harboring Ca^{2+} ligand
766 mutations, were purified in the same manner at the WT C2-domains. Full-length SYT9 was
767 purified as a His_6-SUMO-tagged protein using the pET28 vector.
768

769 **Vesicle Preparation**

770 Protein free liposomes, for co-sedimentation assays, were generated by drying lipids
771 (30% PE and 70% PC; 15% PS, 30% PE, and 55% PC; and 25% PS, 30% PE, and 45% PC) in
772 chloroform, under a stream of nitrogen. The film was rehydrated and suspended by vortexing in
773 50 mM HEPES-NaOH, 100 mM NaCl, pH 7.4, and extruded through 50 nm polycarbonate
774 membranes to generate liposomes (Avanti Polar Lipids, Birmingham, AL, USA). SNARE-
775 bearing vesicles, for *in vitro* fusion assays, were prepared as previously described (Bhalla et al.,
776 2006). Lipid compositions were as follows: 15% PS, 27% PE, 55% PC, 1.5% NBD-PE, and
777 1.5% Rho-PE for SYB2 vesicles, and 25% PS, 30% PE, and 45% PC for SYX1A vesicles.

778

779 ***In vitro* Fusion Assays**

780 Fusion assays between SYB2 and SYX1A vesicles were conducted using a scaled-
781 down version of the referenced method (Bhalla et al., 2006). For split t-SNARE fusion assays, 1
782 μM of the cytoplasmic domain (C2AB) or 2 μM of isolated C2-domains, SYB2 vesicles, SYX1A
783 vesicles, 0.2 mM EGTA, and 7 μM soluble SNAP-25B were incubated for 20 min at 37°C. Ca^{2+}
784 (1 mM final free concentration) was added and the reaction was monitored for an additional 60
785 min. N-dodecyl-β-d-maltoside was added at the end of the experiment, to yield the maximum
786 fluorescence signal. NBD donor fluorescence was monitored using a Synergy HT multi-
787 detection microplate reader (Bio-Tek, Santa Clara, CA, USA). Traces were normalized to the
788 first time point, and the maximum fluorescence signal, to determine the $\%F_{max}$.

789

790 **Co-sedimentation Assays**

791 WT SYT9 C2A, C2B, or C2AB (4 μM) were combined with protein-free liposomes (1 mM
792 total lipid; %PS as indicated in Fig. 6B) in 0.2 mM EGTA or 1 mM Ca^{2+} and incubated for 15 min
793 at RT. Samples were then centrifuged in an Optima MAX-E tabletop ultracentrifuge (Beckman
794 Coulter, Brea, CA, USA) at 184,000 x g (65,000 rpm) for 45 min at 4°C. After centrifugation, the

795 supernatant (S), and the pellet (P) were collected, and equal fractions were subjected to SDS-
796 PAGE and Coomassie blue staining. Bands were quantified by densitometry and plotted.
797
798 **Isothermal Titration Calorimetry (ITC)**
799 WT and CLM forms of the isolated C2-domains of SYT9 were dialyzed overnight in ITC
800 buffer (50 mM HEPES-NaOH, pH 7.4, 200 mM NaCl, and 10% glycerol) in the presence of
801 Chelex-100 resin (BioRad), to remove residual divalent cations. ITC buffer was subsequently
802 filtered and used to make Ca^{2+} and protein dilutions. Heat of binding was measured, using a
803 MicroCal® iTC200 (Malvern Panalytical, Malvern, UK), at 25 °C, in response to twenty injections
804 of Ca^{2+} into the sample cell containing 100 μM protein. Heat of dilution was corrected by
805 subtracting the signal that arises when Ca^{2+} is diluted into buffer. Data were analyzed using the
806 "sequential binding site" model in the data software package.
807
808 **ACKNOWLEDGEMENTS**
809 We would like to thank members of the Chapman lab and K. Bjornson for insightful
810 comments and valuable discussion related to the manuscript. This study was supported by
811 grants from the NIH (MH061876 and NS097362 to E.R.C.). C.S.E. was supported in part by a
812 PhRMA Foundation predoctoral fellowship and by the UW-Madison Molecular and Cellular
813 Pharmacology Training Grant (T32 GM008688). E.R.C. is an Investigator of the Howard Hughes
814 Medical Institute.
815
816 This article is subject to HHMI's Open Access to Publications policy. HHMI lab heads have
817 previously granted a nonexclusive CC BY 4.0 license to the public and a sublicensable license
818 to HHMI in their research articles. Pursuant to those licenses, the author-accepted manuscript
819 of this article can be made freely available under a CC BY 4.0 license immediately upon
820 publication.

AUTHOR CONTRIBUTIONS

M.J.S.: conceptualization, data curation, formal analysis, investigation, methodology, project administration, software, supervision, validation, visualization, writing – original draft, writing – review and editing. C.S.E.: investigation, formal analysis, visualization. K.S.S.: investigation, formal analysis, validation, visualization. Z.W.: investigation, formal analysis, validation. E.R.C.: conceptualization, funding acquisition, methodology, project administration, resources, supervision, visualization, writing – original draft, writing – review and editing.

COMPETING INTERESTS

The authors have no competing interests to declare.

REFERENCES

Almeida, T. A., Rojo, J., Nieto, P. M., Pinto, F. M., Hernandez, M., Martín, J. D., & Candenas, M. L. (2004). Tachykinins and Tachykinin Receptors: Structure and Activity Relationships. *Current Medicinal Chemistry*, *11*(15), 2045–2081. https://doi.org/10.2174/0929867043364748

Angulo, J. A., & McEwen, B. S. (1994). Molecular aspects of neuropeptide regulation and function in the corpus striatum and nucleus accumbens. *Brain Research Reviews*, *19*(1), 1–28. https://doi.org/10.1016/0165-0173(94)90002-7

Bai, H., Xue, R., Bao, H., Zhang, L., Yethiraj, A., Cui, Q., & Chapman, E. R. (2016). Different states of synaptotagmin regulate evoked versus spontaneous release. *Nature Communications*, *7*, 1–9. https://doi.org/10.1038/ncomms10971

Berg, E. A., Johnson, R. J., Leeman, S. E., Boyd, N., Kimerer, L., & Fine, R. E. (2000). Isolation and characterization of substance P-containing dense core vesicles from rabbit optic nerve and termini. *Journal of Neuroscience Research*, *62*(6), 830–839. https://doi.org/10.1002/1097-4547(20001215)62:6<830::AID-JNR10>3.0.CO;2-E

Bhalla, A., Chicka, M. C., & Chapman, E. R. (2008). Analysis of the synaptotagmin family during reconstituted membrane fusion: Uncovering a class of inhibitory isoforms. *Journal of Biological Chemistry*, *283*(31), 21799–21807. https://doi.org/10.1074/jbc.M709628200

Bhalla, A., Chicka, M. C., Tucker, W. C., & Chapman, E. R. (2006). Ca2+-synaptotagmin directly regulates t-SNARE function during reconstituted membrane fusion. *Nature Structural and Molecular Biology*, *13*(4), 323–330. https://doi.org/10.1038/nsmb1076

854 Bhalla, A., Tucker, W. C., & Chapman, E. R. (2005). Synaptotagmin Isoforms Couple Distinct
855 Ranges of Ca2+, Ba2+, and Sr2+ Concentration to SNARE-mediated Membrane Fusion.
856 *Molecular Biology of the Cell*, *16*(10), 4755–4764. https://doi.org/10.1091/mbc.E05-04-
857 0277

858 Bradberry, M. M., & Chapman, E. R. (2022). All-optical monitoring of excitation–secretion
859 coupling demonstrates that SV2A functions downstream of evoked Ca2+ entry. *Journal of*
860 *Physiology*, *600*(3), 645–654. https://doi.org/10.1113/JP282601

861 Brimblecombe, K. R., & Cragg, S. J. (2015). Substance P weights striatal dopamine
862 transmission differently within the striosome-matrix axis. *Journal of Neuroscience*, *35*(24),
863 9017–9023. https://doi.org/10.1523/JNEUROSCI.0870-15.2015

864 Cao, P., Maximov, A., & Südhof, T. C. (2011). Activity-dependent IGF-1 exocytosis is controlled
865 by the Ca 2+-sensor synaptotagmin-10. *Cell*, *145*(2), 300–311.
866 https://doi.org/10.1016/j.cell.2011.03.034

867 Chang, S., Trimbuch, T., & Rosenmund, C. (2018). Synaptotagmin-1 drives synchronous Ca2+
868 -triggered fusion by C2B-domain-mediated synaptic-vesicle-membrane attachment. *Nature*
869 *Neuroscience*, *21*(1), 33–42. https://doi.org/10.1038/s41593-017-0037-5

870 Chapman, E. R. (2008). How does synaptotagmin trigger neurotransmitter release? In *Annual*
871 *Review of Biochemistry* (Vol. 77, pp. 615–641).
872 https://doi.org/10.1146/annurev.biochem.77.062005.101135

873 Chicka, M. C., Hui, E., Liu, H., & Chapman, E. R. (2008). Synaptotagmin arrests the SNARE
874 complex before triggering fast, efficient membrane fusion in response to Ca2+. *Nature*
875 *Structural and Molecular Biology*, *15*(8), 827–835. https://doi.org/10.1038/nsmb.1463

876 Courtney, N. A., Bao, H., Briguglio, J. S., & Chapman, E. R. (2019). Synaptotagmin 1 clamps
877 synaptic vesicle fusion in mammalian neurons independent of complexin. *Nature*
878 *Communications*, *10*(1). https://doi.org/10.1038/s41467-019-12015-w

879 Courtney, N. A., Briguglio, J. S., Bradberry, M. M., Greer, C., & Chapman, E. R. (2018).
880 Excitatory and Inhibitory Neurons Utilize Different Ca2+ Sensors and Sources to Regulate
881 Spontaneous Release. *Neuron*, *98*(5), 977-991.e5.
882 https://doi.org/10.1016/j.neuron.2018.04.022

883 Craxton, M. (2010). A manual collection of Syt, Esyt, Rph3a, Rph3al, Doc2, and Dblc2 genes
884 from 46 metazoan genomes - an open access resource for neuroscience and evolutionary
885 biology. *BMC Genomics*, *11*(1). https://doi.org/10.1186/1471-2164-11-37

886 Das, D., Bao, H., Courtney, K. C., Wu, L., & Chapman, E. R. (2020). Resolving kinetic
887 intermediates during the regulated assembly and disassembly of fusion pores. *Nature*
888 *Communications*, *11*(1), 231. https://doi.org/10.1038/s41467-019-14072-7

889 Dean, C., Dunning, F. M., Liu, H., Bomba-Warczak, E., Martens, H., Bharat, V., Ahmed, S., &
890 Chapman, E. R. (2012). Axonal and dendritic synaptotagmin isoforms revealed by a
891 pHluorin-syt functional screen. *Molecular Biology of the Cell*, *23*(9), 1715–1727.
892 https://doi.org/10.1091/mbc.e11-08-0707

Dean, C., Liu, H., Dunning, F. M., Chang, P. Y., Jackson, M. B., & Chapman, E. R. (2009). Synaptotagmin-IV modulates synaptic function and long-term potentiation by regulating BDNF release. *Nature Neuroscience*, *12*(6), 767–776. https://doi.org/10.1038/nn.2315

Dean, C., Liu, H., Staudt, T., Stahlberg, M. A., Vingill, S., Buckers, J., Kamin, D., Engelhardt, J., Jackson, M. B., Hell, S. W., & Chapman, E. R. (2012). Distinct Subsets of Syt-IV/BDNF Vesicles Are Sorted to Axons versus Dendrites and Recruited to Synapses by Activity. *Journal of Neuroscience*, *32*(16), 5398–5413. https://doi.org/10.1523/JNEUROSCI.4515-11.2012

Deo, C., Sheu, S. H., Seo, J., Clapham, D. E., & Lavis, L. D. (2019). Isomeric Tuning Yields Bright and Targetable Red Ca2+ Indicators. *Journal of the American Chemical Society*, *141*(35), 13734–13738. https://doi.org/10.1021/jacs.9b06092

DiAntonio, A., & Schwarz, T. L. (1994). The effect on synaptic physiology of synaptotagmin mutations in drosophila. *Neuron*, *12*(4), 909–920. https://doi.org/10.1016/0896-6273(94)90342-5

Emptage, N. J., Reid, C. A., & Fine, A. (2001). Calcium stores in hippocampal synaptic boutons mediate short-term plasticity, store-operated Ca2+entry, and spontaneous transmitter release. *Neuron*, *29*(1), 197–208. https://doi.org/10.1016/S0896-6273(01)00190-8

Evans, C. S., He, Z., Bai, H., Lou, X., Jeggle, P., Sutton, R. B., Edwardson, J. M., & Chapman, E. R. (2016). Functional analysis of the interface between the tandem C2 domains of synaptotagmin-1. *Molecular Biology of the Cell*, *27*(6), 979–989. https://doi.org/10.1091/mbc.E15-07-0503

Evans, C. S., Ruhl, D. A., & Chapman, E. R. (2015). An engineered metal sensor tunes the kinetics of synaptic transmission. *Journal of Neuroscience*, *35*(34), 11769–11779. https://doi.org/10.1523/JNEUROSCI.1694-15.2015

Fernández-Alfonso, T., Kwan, R., & Ryan, T. A. (2006). Synaptic Vesicles Interchange Their Membrane Proteins with a Large Surface Reservoir during Recycling. *Neuron*, *51*(2), 179–186. https://doi.org/10.1016/J.NEURON.2006.06.008

Fernández-Chacón, R., Shin, O. H., Königstorfer, A., Matos, M. F., Meyer, A. C., Garcia, J., Gerber, S. H., Rizo, J., Südhof, T. C., & Rosenmund, C. (2002). Structure/function analysis of Ca2+ binding to the C2A domain of synaptotagmin 1. *Journal of Neuroscience*, *22*(19), 8438–8446. https://doi.org/10.1523/jneurosci.22-19-08438.2002

Fukuda, M., Kowalchyk, J. A., Zhang, X., Martin, T. F. J., & Mikoshiba, K. (2002). Synaptotagmin IX regulates Ca2+-dependent secretion in PC12 cells. *Journal of Biological Chemistry*, *277*(7), 4601–4604. https://doi.org/10.1074/jbc.C100588200

Gaffaney, J. D., Dunning, F. M., Wang, Z., Hui, E., & Chapman, E. R. (2008). Synaptotagmin C2B domain regulates Ca2+-triggered fusion in vitro: Critical residues revealed by scanning alanine mutagenesis. *Journal of Biological Chemistry*, *283*(46), 31763–31775. https://doi.org/10.1074/JBC.M803355200

Geppert, M., Goda, Y., Hammer, R. E., Li, C., Rosahl, T. W., Stevens, C. F., & Südhof, T. C. (1994). Synaptotagmin I: A major Ca2+sensor for transmitter release at a central synapse. *Cell*, *79*(4), 717–727. https://doi.org/10.1016/0092-8674(94)90556-8

Gerfen, C. R. (1992). The neostriatal mosaic: multiple levels of compartmental organization. In *Trends in Neurosciences* (Vol. 15, Issue 4, pp. 133–139). Elsevier Current Trends. https://doi.org/10.1016/0166-2236(92)90355-C

Groffen, A. J., Martens, S., Arazola, R. D., Cornelisse, L. N., Lozovaya, N., De Jong, A. P. H., Goriounova, N. A., Habets, R. L. P., Takai, Y., Borst, J. G., Brose, N., McMahon, H. T., & Verhage, M. (2010). Doc2b is a high-affinity Ca2+sensor for spontaneous neurotransmitter release. *Science*, *327*(5973), 1614–1618. https://doi.org/10.1126/science.1183765

Haberman, Y., Grimberg, E., Fukuda, M., & Sagi-Eisenberg, R. (2003). Synaptotagmin IX, a possible linker between the perinuclear endocytic recycling compartment and the microtubules. *Journal of Cell Science*, *116*(21), 4307–4318. https://doi.org/10.1242/jcs.00719

Hamilton, J., Greiner, R., Salem N., J., & Kim, H. Y. (2000). n-3 fatty acid deficiency decreases phosphatidylserine accumulation selectively in neuronal tissues. *Lipids*, *35*(8), 863–869. https://doi.org/10.1007/S11745-000-0595-x

Haneda, E., Higuchi, M., Maeda, J., Inaji, M., Okauchi, T., Ando, K., Obayashi, S., Nagai, Y., Narazaki, M., Ikehira, H., Nakao, R., Zhang, M.-R., Suzuki, K., Suzuki, H., & Suhara, T. (2007). In Vivo Mapping of Substance P Receptors in Brains of Laboratory Animals by High-Resolution Imaging Systems. *Synapse*, *61*(4), 205–215. https://doi.org/10.1002/syn.20363

He, Z.-X., Liu, T.-Y., Yin, Y.-Y., Song, H.-F., & Zhu, X.-J. (2019). Substance P plays a critical role in synaptic transmission in striatal neurons. *Biochemical and Biophysical Research Communications*, *511*(2), 369–373. https://doi.org/S0006291X19302438

Iezzi, M., Eliasson, L., Fukuda, M., & Wollheim, C. B. (2005). Adenovirus-mediated silencing of Synaptotagmin 9 inhibits Ca 2+-dependent insulin secretion in islets. *FEBS Letters*, *579*(23), 5241–5246. https://doi.org/10.1016/j.febslet.2005.08.047

Jorgensen, E. M., Hartweig, E., Schuske, K., Nonet, M. L., Jin, Y., & Horvitz, H. R. (1995). Defective recycling of synaptic vesicles in synaptotagmin mutants of Caenorhabditis elegans. *Nature*, *378*, 196–199. https://doi.org/10.1038/255242a0

Jung, M., Calassi, R., Maruani, J., Barnouin, M., Souilhac, J., Poncelet, M., Gueudet, C., Emondsalt, X., Soubrié, B., Brelière, J., & le Fur, G. (1994). Neuropharmacological characterization of SR 140333, a non peptide antagonist of NK1 receptors. *Neuropharmacology*, *33*(2), 167–179.

Kemp, J. M., & Powell, T. P. (1971). The structure of the caudate nucleus of the cat: light and electron microscopy. *Philosophical Transactions of the Royal Society of London. Series B, Biological Sciences*, *262*(845), 383–401. https://doi.org/10.1098/rstb.1971.0102

Kerr, A. M., Reisinger, E., & Jonas, P. (2008). Differential dependence of phasic transmitter release on synaptotagmin 1 at GABAergic and glutamatergic hippocampal synapses. *Proceedings of the National Academy of Sciences of the United States of America*, *105*(40), 15581–15586. https://doi.org/10.1073/pnas.0800621105

973 Kochubey, O., Babai, N., & Schneggenburger, R. (2016). A Synaptotagmin Isoform Switch
974 during the Development of an Identified CNS Synapse. *Neuron*, *90*(5), 984–999.
975 https://doi.org/10.1016/j.neuron.2016.04.038

976 Koos, T., Tepper, J. M., & Wilson, C. J. (2004). Comparison of IPSCs evoked by spiny and fast-
977 spiking neurons in the neostriatum. *Journal of Neuroscience*, *24*(36), 7916–7922.
978 https://doi.org/10.1523/JNEUROSCI.2163-04.2004

979 Krause, J. E., Chirgwin, J. M., Carter, M. S., Xu, Z. S., & Hershey, A. D. (1987). Three rat
980 preprotachykinin mRNAs encode the neuropeptides substance P and neurokinin A.
981 *Proceedings of the National Academy of Sciences of the United States of America*, *84*(3),
982 881–885. https://doi.org/10.1073/pnas.84.3.881

983 Kügler, S., Kilic, E., & Bähr, M. (2003). Human synapsin 1 gene promoter confers highly neuron-
984 specific long-term transgene expression from an adenoviral vector in the adult rat brain
985 depending on the transduced area. In *Gene Therapy* (Vol. 10, Issue 4, pp. 337–347).
986 https://doi.org/10.1038/sj.gt.3301905

987 Ladner, C. L., Yang, J., Turner, R. J., & Edwards, R. A. (2004). Visible fluorescent detection of
988 proteins in polyacrylamide gels without staining. *Analytical Biochemistry*, *326*(1), 13–20.
989 https://doi.org/10.1016/j.ab.2003.10.047

990 Littleton, J. T., Stern, M., Perin, M., & Bellen, H. J. (1994). Calcium dependence of
991 neurotransmitter release and rate of spontaneous vesicle fusions are altered in Drosophila
992 synaptotagmin mutants. *Proceedings of the National Academy of Sciences of the United*
993 *States of America*, *91*(23), 10888–10892. https://doi.org/10.1073/pnas.91.23.10888

994 Liu, H., Bai, H., Xue, R., Takahashi, H., Edwardson, J. M., & Chapman, E. R. (2014). Linker
995 mutations reveal the complexity of synaptotagmin 1 action during synaptic transmission.
996 *Nature Neuroscience*, *17*(5), 670–677. https://doi.org/10.1038/nn.3681

997 Liu, H., Dean, C., Arthur, C. P., Dong, M., & Chapman, E. R. (2009). Autapses and networks of
998 hippocampal neurons exhibit distinct synaptic transmission phenotypes in the absence of
999 synaptotagmin I. *Journal of Neuroscience*, *29*(23), 7395–7403.
1000 https://doi.org/10.1523/JNEUROSCI.1341-09.2009

1001 Lois, C., Hong, E. J., Pease, S., Brown, E. J., & Baltimore, D. (2002). Germline transmission
1002 and tissue-specific expression of transgenes delivered by lentiviral vectors. *Science*,
1003 *295*(5556), 868–872. https://doi.org/10.1126/science.1067081

1004 Lynch, K. L., & Martin, T. F. J. (2007). Synaptotagmins I and IX function redundantly in
1005 regulated exocytosis but not endocytosis in PC12 cells. *Journal of Cell Science*, *120*(4),
1006 617–627. https://doi.org/10.1242/jcs.03375

1007 Maximov, A., & Südhof, T. C. (2005). Autonomous Function of Synaptotagmin 1 in Triggering
1008 Synchronous Release Independent of Asynchronous Release. *Neuron*, *48*(4), 547–554.
1009 https://doi.org/10.1016/J.NEURON.2005.09.006

1010 Miesenböck, G., de Angelis, D. A., & Rothman, J. E. (1998). Visualizing secretion and synaptic
1011 transmission with pH-sensitive green fluorescent proteins. *Nature*, *394*(6689), 192–195.

1012 Mittelsteadt, T., Seifert, G., Alvárez-Barón, E., Steinhäuser, C., Becker, A. J., & Schoch, S.
1013 (2009). Differential mRNA expression patterns of the synaptotagmin gene family in the
1014 rodent brain. In *Journal of Comparative Neurology* (Vol. 512, Issue 4, pp. 514–528).
1015 https://doi.org/10.1002/cne.21908

1016 Moro, A., Hoogstraaten, R. I., Persoon, C. M., Verhage, M., & Toonen, R. F. (2021).
1017 Quantitative analysis of dense-core vesicle fusion in rodent CNS neurons. *STAR Protocols*,
1018 *2*(1), 100325. https://doi.org/10.1016/j.xpro.2021.100325

1019 Nicholson-Tomishima, K., & Ryan, T. A. (2004). Kinetic efficiency of endocytosis at mammalian
1020 CNS synapses requires synaptotagmin I. *Proceedings of the National Academy of*
1021 *Sciences of the United States of America*, *101*(47), 16648–16652.
1022 https://doi.org/10.1073/pnas.0406968101

1023 Nishiki, T. I., & Augustine, G. J. (2004). Dual roles of the C2B domain of synaptotagmin I in
1024 synchronizing Ca2+-dependent neurotransmitter release. *Journal of Neuroscience*, *24*(39),
1025 8542–8550. https://doi.org/10.1523/JNEUROSCI.2545-04.2004

1026 Pang, Z. P., Melicoff, E., Padgett, D., Liu, Y., Teich, A. F., Dickey, B. F., Lin, W., Adachi, R., &
1027 Südhof, T. C. (2006). Synaptotagmin-2 is essential for survival and contributes to Ca 2+
1028 triggering of neurotransmitter release in central and neuromuscular synapses. *Journal of*
1029 *Neuroscience*, *26*(52), 13493–13504. https://doi.org/10.1523/JNEUROSCI.3519-06.2006

1030 Pang, Z. P., Shin, O. H., Meyer, A. C., Rosenmund, C., & Südhof, T. C. (2006). A gain-of-
1031 function mutation in synaptotagmin-1 reveals a critical role of Ca2+-dependent soluble N-
1032 ethylmaleimide-sensitive factor attachment protein receptor complex binding in synaptic
1033 exocytosis. *Journal of Neuroscience*, *26*(48), 12556–12565.
1034 https://doi.org/10.1523/JNEUROSCI.3804-06.2006

1035 Persoon, C. M., Moro, A., Nassal, J. P., Farina, M., Broeke, J. H., Arora, S., Dominguez, N.,
1036 Weering, J. R., Toonen, R. F., & Verhage, M. (2018). Pool size estimations for dense-core
1037 vesicles in mammalian CNS neurons. *The EMBO Journal*, *37*(20).
1038 https://doi.org/10.15252/embj.201899672

1039 Poskanzer, K. E., Marek, K. W., Sweeney, S. T., & Davis, G. W. (2003). Synaptotagmin I is
1040 necessary for compensatory synaptic vesicle endocytosis in vivo. *Nature*, *426*(6966), 559–
1041 563.

1042 Quadros, R. M., Miura, H., Harms, D. W., Akatsuka, H., Sato, T., Aida, T., Redder, R.,
1043 Richardson, G. P., Inagaki, Y., Sakai, D., Buckley, S. M., Seshacharyulu, P., Batra, S. K.,
1044 Behlke, M. A., Zeiner, S. A., Jacobi, A. M., Izu, Y., Thoreson, W. B., Urness, L. D., …
1045 Gurumurthy, C. B. (2017). Easi-CRISPR: A robust method for one-step generation of mice
1046 carrying conditional and insertion alleles using long ssDNA donors and CRISPR
1047 ribonucleoproteins. *Genome Biology*, *18*(1), 1–15. https://doi.org/10.1186/s13059-017-
1048 1220-4

1049 Radhakrishnan, A., Li, X., Grushin, K., Krishnakumar, S. S., Liu, J., & Rothman, J. E. (2021).
1050 Symmetrical arrangement of proteins under release-ready vesicles in presynaptic
1051 terminals. *Proceedings of the National Academy of Sciences of the United States of*
1052 *America*, *118*(5). https://doi.org/10.1073/pnas.2024029118

1053 Radhakrishnan, A., Stein, A., Jahn, R., & Fasshauer, D. (2009). The Ca2+ affinity of
1054 synaptotagmin 1 is markedly increased by a specific interaction of its C2B domain with
1055 phosphatidylinositol 4,5-bisphosphate. *Journal of Biological Chemistry*, *284*(38), 25749–
1056 25760. https://doi.org/10.1074/jbc.M109.042499

1057 Rao, T. C., Passmore, D. R., Peleman, A. R., Das, M., Chapman, E. R., & Anantharam, A.
1058 (2014). Distinct fusion properties of synaptotagmin-1 and synaptotagmin-7 bearing dense
1059 core granules. *Molecular Biology of the Cell*, *25*(16), 2416–2427.
1060 https://doi.org/10.1091/mbc.E14-02-0702

1061 Reist, N. E., Buchanan, J., Li, J., DiAntonio, A., Buxton, E. M., & Schwarz, T. L. (1998).
1062 Morphologically docked synaptic vesicles are reduced in synaptotagmin mutants of
1063 Drosophila. *Journal of Neuroscience*, *18*(19), 7662–7673.
1064 https://doi.org/10.1523/jneurosci.18-19-07662.1998

1065 Rickman, C., Craxton, M., Osborne, S., & Davletov, B. (2004). Comparative analysis of tandem
1066 C2 domains from the mammalian synaptotagmin family. *Biochemical Journal*, *378*(2), 681–
1067 686. https://doi.org/10.1042/bj20031407

1068 Roper, L. K., Briguglio, J. S., Evans, C. S., Jackson, M. B., & Chapman, E. R. (2015). Sex-
1069 specific regulation of follicle-stimulating hormone secretion by synaptotagmin 9. *Nature*
1070 *Communications*, *6*, 1–10. https://doi.org/10.1038/ncomms9645

1071 Schindelin, J., Arganda-Carreras, I., Frise, E., Kaynig, V., Longair, M., Pietzsch, T., Preibisch,
1072 S., Rueden, C., Saalfeld, S., Schmid, B., Tinevez, J. Y., White, D. J., Hartenstein, V.,
1073 Eliceiri, K., Tomancak, P., & Cardona, A. (2012). Fiji: An open-source platform for
1074 biological-image analysis. *Nature Methods*, *9*(7), 676–682.
1075 https://doi.org/10.1038/nmeth.2019

1076 Schmitz, S. K., Hjorth, J. J. J., Joemai, R. M. S., Wijntjes, R., Eijgenraam, S., de Bruijn, P.,
1077 Georgiou, C., de Jong, A. P. H., van Ooyen, A., Verhage, M., Cornelisse, L. N., Toonen, R.
1078 F., & Veldkamp, W. (2011). Automated analysis of neuronal morphology, synapse number
1079 and synaptic recruitment. *Journal of Neuroscience Methods*, *195*(2), 185–193.
1080 https://doi.org/10.1016/J.JNEUMETH.2010.12.011

1081 Shin, O. H., Maximov, A., Lim, B. K., Rizo, J., & Südhof, T. C. (2004). Unexpected Ca2+-binding
1082 properties of synaptotagmin 9. *Proceedings of the National Academy of Sciences of the*
1083 *United States of America*, *101*(8), 2554–2559. https://doi.org/10.1073/pnas.0308477100

1084 Shin, O. H., Xu, J., Rizo, J., & Südhof, T. C. (2009). Differential but convergent functions of
1085 Ca2+ binding to synaptotagmin-1 C2 domains mediate neurotransmitter release.
1086 *Proceedings of the National Academy of Sciences of the United States of America*,
1087 *106*(38), 16469–16474. https://doi.org/10.1073/PNAS.0908798106

1088 Shults, C. W., Quirion, R., Chronwall, B., Chase, T. N., & O'Donohue, T. L. (1984). A
1089 comparison of the anatomical distribution of substance P and substance P receptors in the
1090 rat central nervous system. *Peptides*, *5*(6), 1097–1128. https://doi.org/10.1016/0196-
1091 9781(84)90177-3

1092 Simkus, C. R. L., & Stricker, C. (2002). The contribution of intracellular calcium stores to
1093 mEPSCs recorded in layer II neurones of rat barrel cortex. *Journal of Physiology*, *545*(2),
1094 521–535. https://doi.org/10.1113/jphysiol.2002.022103

1095 Stevens, C. F., & Sullivan, J. M. (2003). The synaptotagmin C2A domain is part of the calcium
1096 sensor controlling fast synaptic transmission. *Neuron*, *39*(2), 299–308.
1097 https://doi.org/10.1016/S0896-6273(03)00432-X

1098 Sutton, R. B., Davletov, B. A., Berghuis, A. M., Südhof, T. C., & Sprang, S. R. (1995). Structure
1099 of the first C2 domain of synaptotagmin I: A novel Ca2+/phospholipid-binding fold. *Cell*,
1100 *80*(6), 929–938. https://doi.org/10.1016/0092-8674(95)90296-1

1101 Takamori, S., Holt, M., Stenius, K., Lemke, E. A., Grønborg, M., Riedel, D., Urlaub, H., Schenck,
1102 S., Brügger, B., Ringler, P., Müller, S. A., Rammner, B., Gräter, F., Hub, J. S., De Groot, B.
1103 L., Mieskes, G., Moriyama, Y., Klingauf, J., Grubmüller, H., … Jahn, R. (2006). Molecular
1104 Anatomy of a Trafficking Organelle. *Cell*, *127*(4), 831–846.
1105 https://doi.org/10.1016/j.cell.2006.10.030

1106 Taoufiq, Z., Ninov, M., Villar-Briones, A., Wang, H. Y., Sasaki, T., Roy, M. C., Beauchain, F.,
1107 Mori, Y., Yoshida, T., Takamori, S., Jahn, R., & Takahashi, T. (2020). Hidden proteome of
1108 synaptic vesicles in the mammalian brain. *Proceedings of the National Academy of*
1109 *Sciences of the United States of America*, *117*(52), 33586–33596.
1110 https://doi.org/10.1073/PNAS.2011870117

1111 Tunstall, M. J., Oorschot, D. E., Kean, A., & Wickens, J. R. (2002). Inhibitory interactions
1112 between spiny projection neurons in the rat striatum. *Journal of Neurophysiology*, *88*(3),
1113 1263–1269. https://doi.org/10.1152/jn.2002.88.3.1263

1114 Ubach, J., Zhang, X., Shao, X., Südhof, T. C., & Rizo, J. (1998). Ca2+ binding to
1115 synaptotagmin: How many Ca2+ ions bind to the tip of a C2-domain? *EMBO Journal*,
1116 *17*(14), 3921–3930. https://doi.org/10.1093/emboj/17.14.3921

1117 Van Den Bogaart, G., Thutupalli, S., Risselada, J. H., Meyenberg, K., Holt, M., Riedel, D.,
1118 Diederichsen, U., Herminghaus, S., Grubmüller, H., & Jahn, R. (2011). Synaptotagmin-1
1119 may be a distance regulator acting upstream of SNARE nucleation. *Nature Structural and*
1120 *Molecular Biology*, *18*(7), 805–812. https://doi.org/10.1038/nsmb.2061

1121 van Westen, R., Poppinga, J., Díez Arazola, R., Toonen, R. F., & Verhage, M. (2021).
1122 Neuromodulator release in neurons requires two functionally redundant calcium sensors.
1123 *Proceedings of the National Academy of Sciences*, *118*(18), 1–12.
1124 https://doi.org/10.1073/pnas.2012137118

1125 Vevea, J. D., & Chapman, E. R. (2020). Acute disruption of the synaptic vesicle membrane
1126 protein synaptotagmin 1 using knockoff in mouse hippocampal neurons. *ELife*, *9*, 1–24.
1127 https://doi.org/10.7554/eLife.56469

1128 Wang, C. T., Grishanin, R., Earles, C. A., Chang, P. Y., Martin, T. F. J., Chapman, E. R., &
1129 Jackson, M. B. (2001). Synaptotagmin modulation of fusion pore kinetics in regulated
1130 exocytosis of dense-core vesicles. *Science*, *294*(5544), 1111–1115.
1131 https://doi.org/10.1126/SCIENCE.1064002

Wolfes, A. C., & Dean, C. (2020). The diversity of synaptotagmin isoforms. In *Current Opinion in Neurobiology* (Vol. 63, pp. 198–209). Elsevier Ltd. https://doi.org/10.1016/j.conb.2020.04.006

Xu, J., Mashimo, T., & Südhof, T. C. (2007). Synaptotagmin-1, -2, and -9: Ca2+ Sensors for Fast Release that Specify Distinct Presynaptic Properties in Subsets of Neurons. *Neuron*, *54*(4), 567–581. https://doi.org/10.1016/j.neuron.2007.05.004

Xu, J., Pang, Z. P., Shin, O. H., & Südhof, T. C. (2009). Synaptotagmin-1 functions as a Ca2+ sensor for spontaneous release. *Nature Neuroscience*, *12*(6), 759–766. https://doi.org/10.1038/nn.2320

Yao, J., Kwon, S. E., Gaffaney, J. D., Dunning, F. M., & Chapman, E. R. (2012). Uncoupling the roles of synaptotagmin I during endo- and exocytosis of synaptic vesicles. *Nature Neuroscience*, *15*(2), 243–249. https://doi.org/10.1038/nn.3013

Zhou, Q., Zhou, P., Wang, A. L., Wu, D., Zhao, M., Südhof, T. C., & Brunger, A. T. (2017). The primed SNARE-complexin-synaptotagmin complex for neuronal exocytosis. *Nature*, *548*(7668), 420–425. https://doi.org/10.1038/nature23484

SUPPLEMENTARY MATERIALS

Thermodynamic properties of Ca^{2+} binding to isolated C2 domains of SYT9 using ITC

	K_D (mM)	DH (cal/mol)	DS (cal/mol/K)	DG (kcal/mol)
SYT9 C2A	K_{D1}= 53.0 ± 8.6	DH_1= 285 ± 65	DS_1= 20.6 ± 0.49	DG_1= -5.85 ± 0.08
	K_{D2}= 182 ± 39	DH_2= 230 ± 220	DS_2= 18.0 ± 1.1	DG_2= -5.14 ± 0.12
	K_{D3}= 337 ± 80	DH_3= 701 ± 250	DS_3= 18.5 ± 0.50	DG_3= -4.79 ± 0.15
SYT9 C2B	K_{D1}= 42.9 ± 5.5	DH_1= -403 ± 20	DS_1= 18.7 ± 0.30	DG_1= -5.97 ± 0.07
	K_{D2}= 500 ± 95	DH_2= -878 ± 78	DS_2= 12.3 ± 0.58	DG_2= -4.53 ± 0.10

Supplementary Table 1

Thermodynamic properties of Ca^{2+} binding to the isolated C2A and C2B domains of SYT9 as determined using ITC. Representative traces of SYT9 C2-domain•Ca^{2+} titrations are shown in (**Fig. 6c**). Data presented as mean ± SEM, *n* = 4.

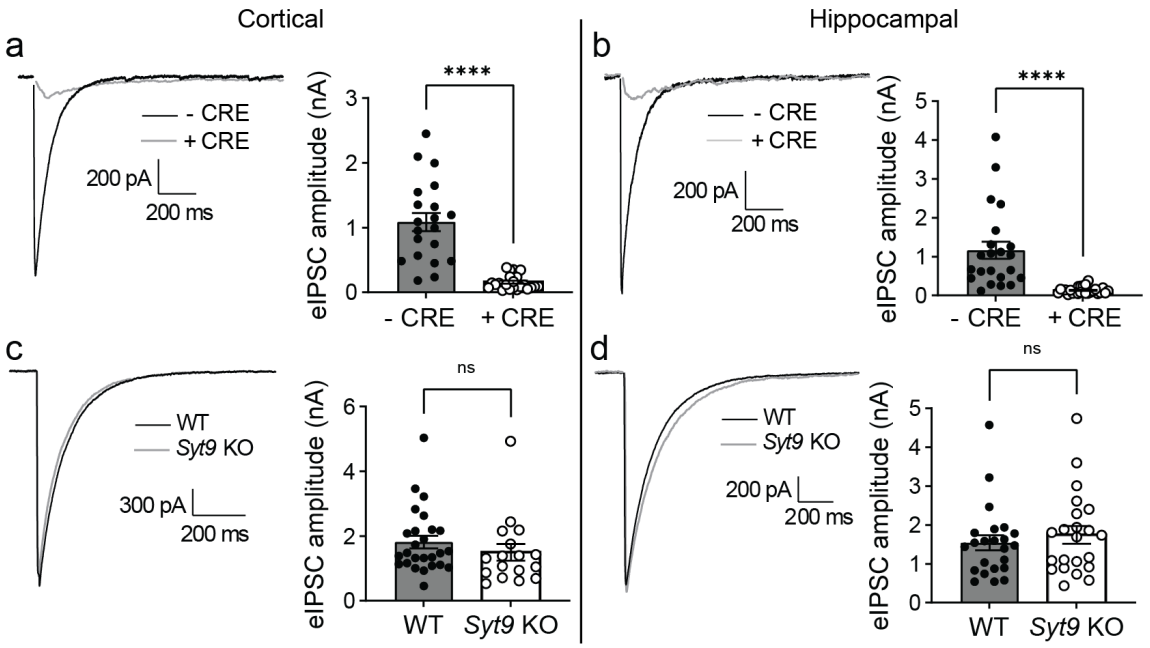

Supplementary Figure 1. SYT1, but not SYT9, supports evoked neurotransmitter release in cortical and hippocampal neurons. a-b*,* Averaged eIPSC traces recorded from WT and *Syt1* cKO cortical (- CRE n = 26; + CRE n = 17) (**a**) and hippocampal (- CRE n = 23; + CRE n = 22) (**b**) neurons with quantification of peak eIPSC amplitude. **c-d**, Same as (**a-b**), but using *Syt9* KO neurons; cortical neurons (WT n = 20; KO n = 23); hippocampal neurons (WT n = 22; KO n = 26). eIPSCs were unaffected in *Syt9 KO* cortical ($p = 0.3231$; unpaired t-test) and hippocampal neurons ($p = 0.4966$; unpaired t-test). In contrast, eIPSCs were disrupted in *Syt1* cKO + CRE cortical ($p < 0.0001$; unpaired t-test) and hippocampal neurons ($p < 0.0001$; unpaired t-test).

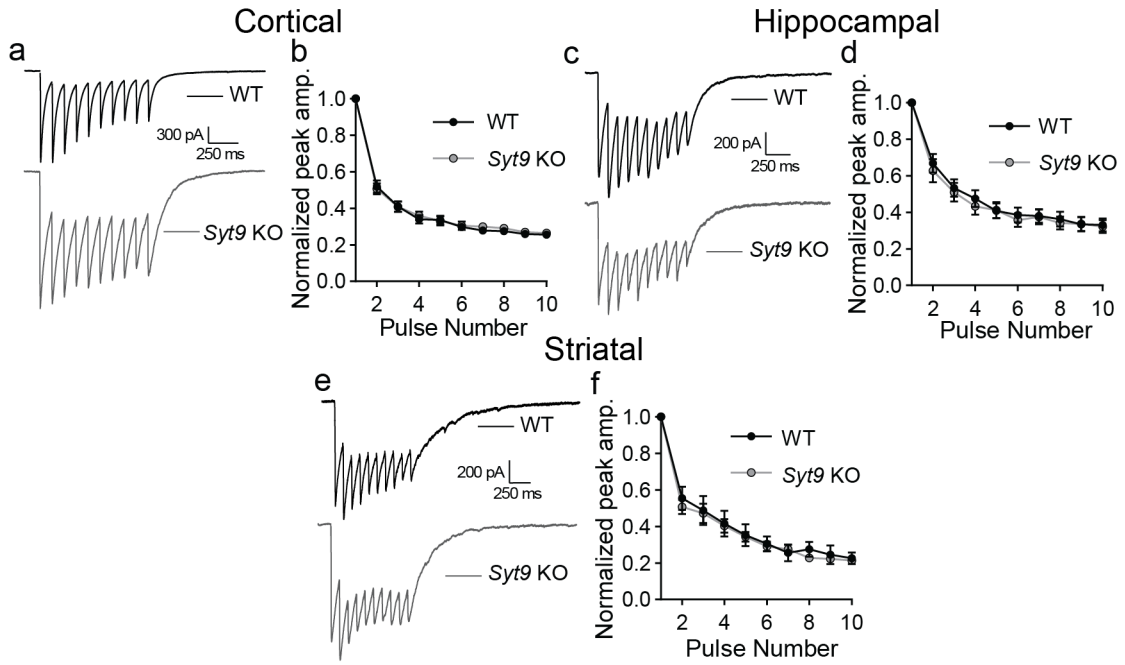

Supplementary Figure 2. Synaptic depression was unchanged in *Syt9* KO cortical, hippocampal, and striatal neurons. a, Averaged 10 Hz eIPSC traces from WT (n = 21) and *Syt9* KO (n = 21) cortical neurons. **b**, Quantification of peak amplitudes from each pulse normalized to the first pulse, showing no difference in short-term plasticity. **c**-**d**, Same as **a**-**b**, but with hippocampal neurons (WT n = 17; KO n = 17). **e**-**f**, Same as **a**-**b**, but with striatal neurons (WT n = 35; KO n = 38). Error bars indicate SEM.

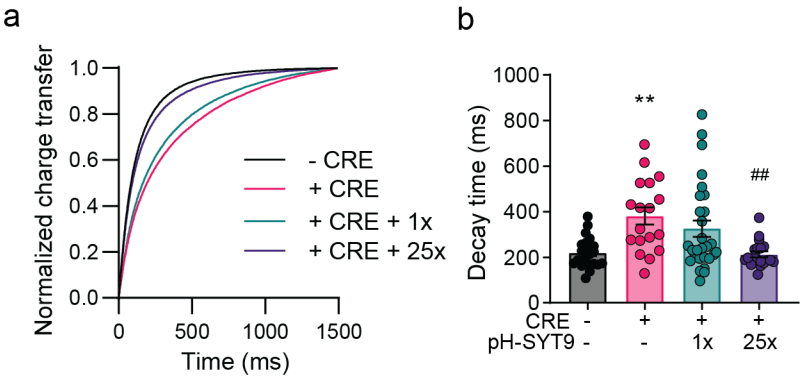

Supplementary Figure 3. eIPSC charge transfer and decay kinetics recorded from *Syt1* cKO cortical neurons expressing pH-SYT9. a, Plot of normalized cumulative charge transfer of - CRE, + CRE, + CRE + 1x pH-SYT9, and + CRE + 25x pH-SYT9 conditions. **b**, Plot of mean decay time (90%-10%) for each condition; 25x fully rescues the decay time, while 1x fails to rescue. Further decay analysis was not performed due to receptor-dominated decay kinetics of

IPSCs in cultured neurons. In this figure, asterisks (*) indicate statistical comparisons (one-way ANOVA with Šídák's multiple comparisons test) to *Syt1* cKO neurons without CRE; hash symbols (#) indicate statistical comparisons to *Syt1* cKO neurons + CRE, where ##p < 0.01.

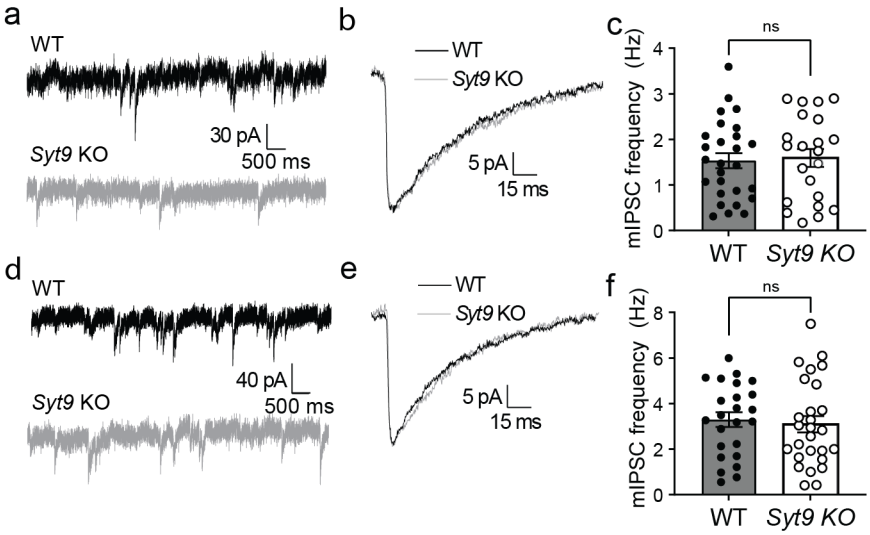

Supplementary Figure 4. mIPSC frequency is unaltered in cultured *Syt9* KO cortical and hippocampal neurons. A, Representative mIPSC traces recorded from WT (n = 27) and *Syt9* KO (n = 22) cortical neurons. **B**, Overlay of averaged mIPSCs, revealing no apparent change in kinetics or amplitude. **C**, mIPSC frequency was unaltered in *Syt9* KO cortical neurons (p = 0.8181; unpaired t-test) **d-f**, Same as **a-c**, but using hippocampal neurons (WT n = 24; KO n = 27) (p = 0.6836; unpaired t-test).

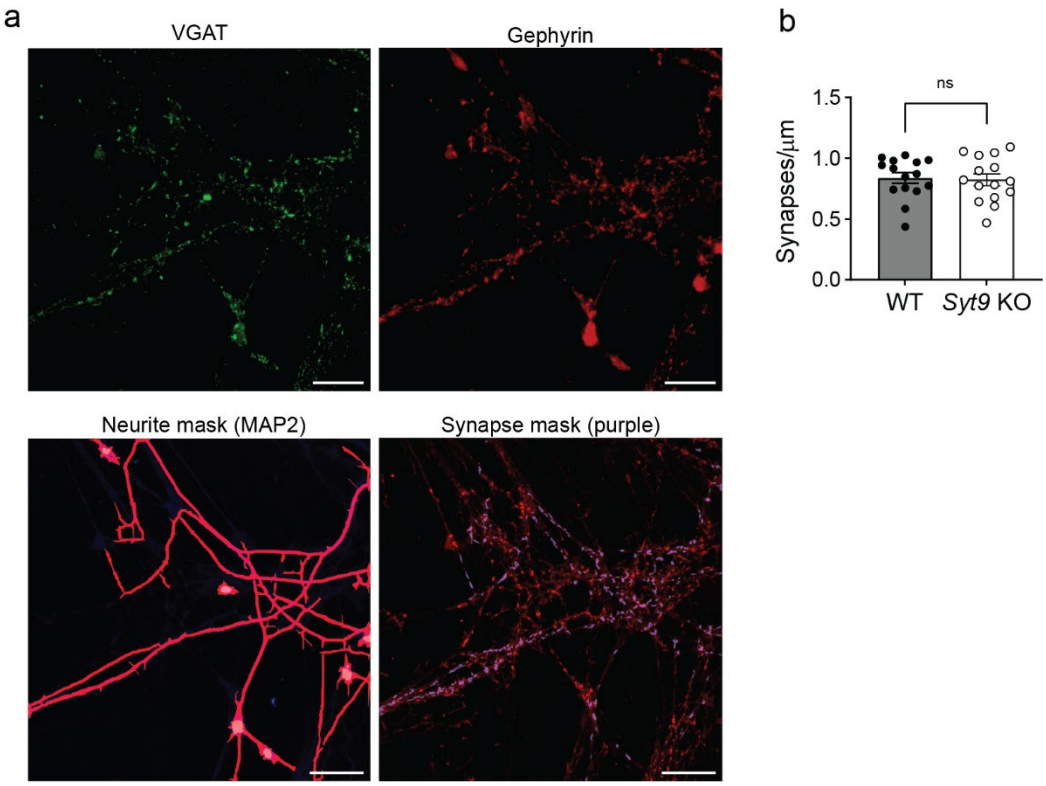

1210

1211 **Supplementary Figure 5. Unchanged synaptic density in *Syt9* KO striatal neurons. a**,
1212 Representative images of cultured striatal neurons stained with α-Gephyrin (red) and α-VGAT
1213 (green) antibodies with a neurite mask generated from MAP2 staining (magenta). Gephyrin and
1214 VMAT overlap within the neurite mask were counted (purple puncta within synapse mask).
1215 Scale bars represent 20 µm. **b**, Number of synapses per µm is unaltered in cultured *Syt9* striatal
1216 neurons (n = 15) compared to WT neurons (n = 15) (p = 0.8212; unpaired t-test).
1217
1218
1219
1220

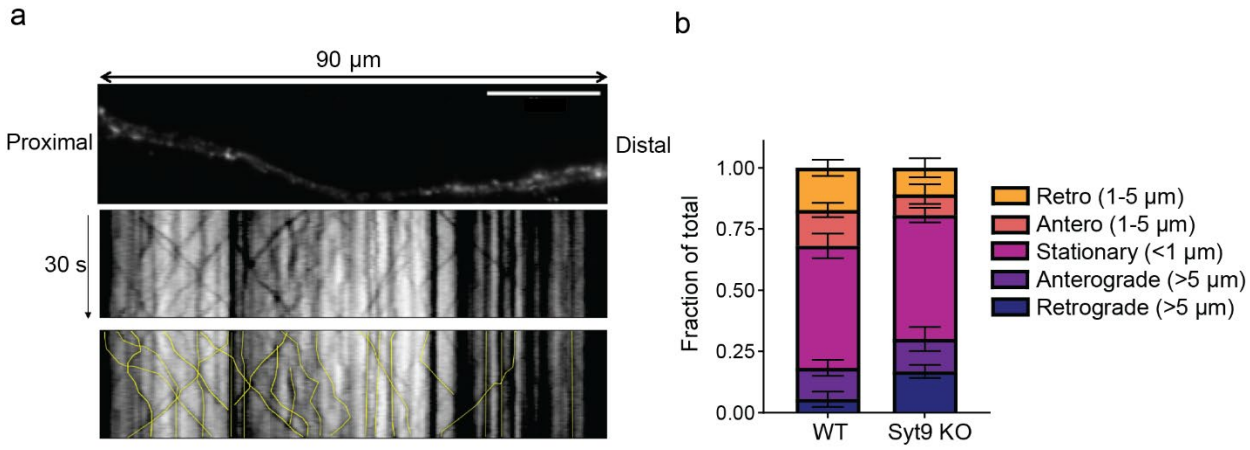

1221

Supplementary Figure 6. The trafficking of SP-pH-bearing DCVs is unaltered in *Syt9* KO striatal neurons. a, *Upper panel*: Representative image of a 90 µm region of a striatal neuron transfected with SP-pH; image was captured after perfusion with NH_4Cl. *Lower panels*: Color inverted kymographs of this region, over a 30 s time period; each track in the kymograph was traced and quantified in the bottom panel (yellow lines). **b**, Quantification of the displacement and direction of SP-pH vesicles. No significant differences in WT (n = 98 vesicles, from 5 cells) versus *Syt9* KO (n = 101 vesicles, from 5 cells) striatal neurons were detected.

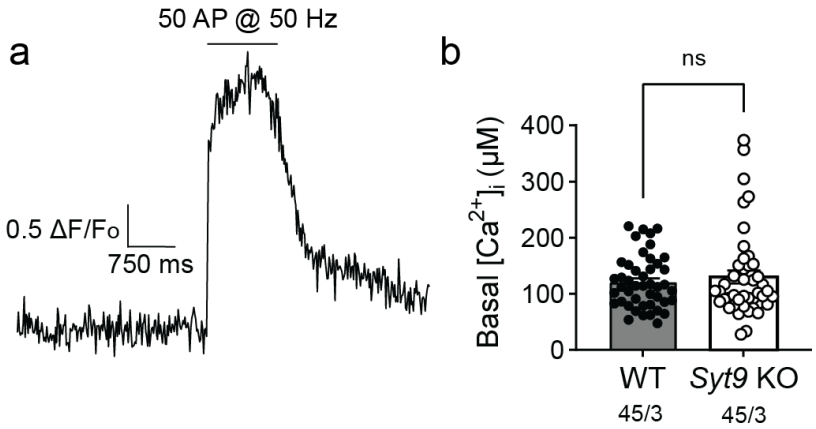

Supplementary Figure 7. Basal presynaptic $[Ca^{2+}]_i$ is unchanged in *Syt9* KO striatal neurons. a, In each trial, the baseline signal was recorded for 3 s, followed by high-frequency train stimulation to obtain the maximal fluorescence of the indicator, to calculate the basal $[Ca^{2+}]_i$ (see Methods). **b**, Basal presynaptic $[Ca^{2+}]_i$ in 1.5 mM $[Ca^{2+}]_e$ did not differ between WT (n = 45) and *Syt9* KO (n = 44) striatal neurons (p = 0.8735; Mann-Whitney test).

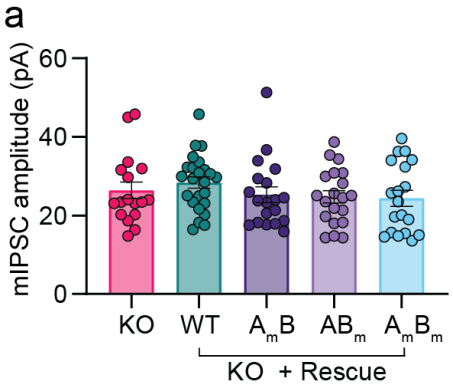

1244 **Supplementary Figure 8. mIPSC amplitude is unaltered in SYT9 CLM rescue. a**, mIPSC
1245 amplitudes measured from (**Fig. 7**). No significant differences in average amplitudes between
1246 conditions were measured (p = 0.4169; Kruskal Wallis test).

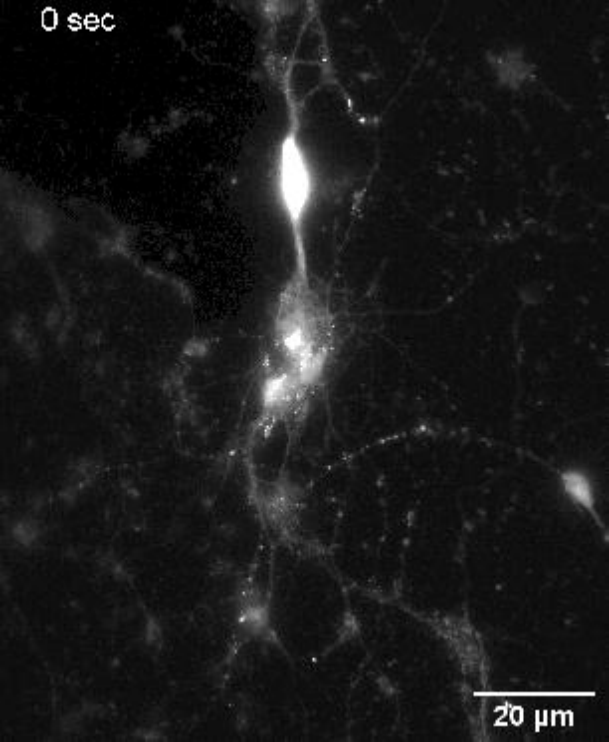
0 sec
20 µm